Published in final edited form as:

Eur J Immunol. 2018 September ; 48(9): 1522–1538. doi:10.1002/eji.201847583.

Sca-1⁺ cardiac fibroblasts promote development of heart failure

Guobao Chen[1], **William Bracamonte-Baran**[1], **Nicola L. Diny**[2], **Xuezhou Hou**[2], **Monica V. Talor**[1], **Kai Fu**[3], **Yue Liu**[3], **Giovanni Davogustto**[4], **Hernan Vasquez**[4], **Heinrich Taegtmeyer**[4], **O. Howard Frazier**[5], **Ari Waisman**[6], **Simon J. Conway**[7], **Fengyi Wan**[3,8], **Daniela Čiháková**[1,2]

[1]Department of Pathology, School of Medicine, Johns Hopkins University, Baltimore, MD, USA

[2]W. Harry Feinstone Department of Molecular Microbiology and Immunology, Bloomberg School of Public Health, Johns Hopkins University, Baltimore, MD, USA

[3]Department of Biochemistry and Molecular Biology, Bloomberg School of Public Health, Johns Hopkins University, Baltimore, MD, USA

[4]Department of Internal Medicine, Division of Cardiology, McGovern Medical School at The University of Texas Health Science Center at Houston, Houston, TX, USA

[5]Texas Heart Institute, CHI St. Luke's Health - Baylor St. Luke's Medical Center, MC 2–114A, PO Box 20345, Houston, TX, USA

[6]Institute for Molecular Medicine, University of Mainz, Mainz, Germany

[7]Wells Center for Pediatric Research, Indiana University School of Medicine, Indianapolis, IN, USA

[8]Department of Oncology, Johns Hopkins University School of Medicine, Baltimore, MD, USA

Abstract

The causative effect of GM-CSF produced by cardiac fibroblasts to development of heart failure has not been shown. We identified the pathological GM-CSF-producing cardiac fibroblast subset and the specific deletion of IL-17A signaling to these cells attenuated cardiac inflammation and heart failure. We describe here the CD45−CD31−CD29^{+}mEFSK4^{+}PDGFRα^{+}Sca-1^{+}periostin^{+} (Sca-1^{+}) cardiac fibroblast subset as the main GM-CSF producer in both experimental autoimmune myocarditis and myocardial infarction mouse models. Specific ablation of IL-17A signaling to Sca-1^{+}periostin^{+} cardiac fibroblasts (Postn^{Cre}Il17ra$^{fl/fl}$) protected mice from post-infarct heart failure and death. Moreover, Postn^{Cre}Il17ra$^{fl/fl}$ mice had significantly fewer GM-CSF-producing Sca-1^{+} cardiac fibrob-lasts and inflammatory Ly6Chi monocytes in the heart. Sca-1^{+} cardiac fibroblasts were not only potent GM-CSF producers, but also exhibited plasticity and switched their cytokine production profiles depending on local microenvironments. Moreover, we also found GMCSF-positive cardiac fibroblasts in cardiac biopsy samples from heart failure patients of myocarditis or ischemic origin. Thus, this is the first identification of a pathological GMCSF-producing cardiac fibroblast subset in human and mice hearts with myocarditis and

correspondence: Dr. Daniela Čiháková Department of Pathology, Johns Hopkins University School of Medicine, 720 Rutland Ave, Ross 648, Baltimore, MD 21205, USA, Fax: +1-410-614-3548, dcihako1@jhmi.edu.

Additional supporting information may be found online in the Supporting Information section at the end of the article.

Conflict of interest: The authors have declared no financial or commercial conflict of interest.

ischemic cardiomyopathy. Sca-1^{+} cardiac fibroblasts direct the type of immune cells infiltrating the heart during cardiac inflammation and drive the development of heart failure.

Keywords

GM-CSF; Heart failure; IL-17; Fibroblasts; Myocarditis

Introduction

Heart failure is a global public health issue with high morbidity and mortality rates, affecting about 26 million people worldwide [1]. The heart failure survival rate is 50% after 5 years and 10% after 10 years in USA [2, 3]. In contrast to other common cardiovascular diseases, heart failure prognoses have shown only modest improvement [4]. The pathophysiology of heart failure is complex and could be triggered by direct injury to the myocardium, such as coronary artery disease and myocardial infarction (MI), or an inflammatory disease state such as myocarditis that leads to inflammatory dilated cardiomyopathy (DCMi) [5–9].

Studies from our lab and others on both myocarditis and MI mouse models revealed that interleukin (IL)-17A, a hallmark cytokine of T helper (Th) 17 cells, plays an important role during post-injury cardiac inflammation and drives the development of heart failure [10, 11]. We found that IL-17A signaling to cardiac fibroblasts, not to immune cells, is essential in the development of heart failure in an experimental autoimmune myocarditis (EAM) mouse model [12]. We showed that IL-17A induced cardiac fibroblasts to produce myelotropic cytokines and chemokines, such as granulocyte macrophage colony-stimulating factor (GM-CSF) and C-C motif chemokine ligand 2 (CCL2, also known as monocyte chemoattractant protein-1), to modulate the immune responses during cardiac inflammation [12]. Others have also reported that cardiac fibroblasts produce GM-CSF and drive the pathology in Kawasaki disease and MI [13, 14].

Despite being often considered as a single homogenous cell population, cardiac fibroblasts are an ambiguously defined cluster of heterogeneous cell populations [15–17]. During embryonic development epicardial cells undergo an epithelial-tomesenchymal transition to become epicardial-derived cells, which penetrate the myocardium to become cardiac fibroblasts [18–20]. Some epicardial-derived cells stay at the sub-epicardial region as mesenchymal stem cells [21–23]. These mesenchymal stem cells remain quiescent and differentiate into cardiac fibroblasts only in response to injury [22, 23]. Another possible source of cardiac fibroblasts are fibrocytes, which are monocyte-like collagen-producing cells derived from bone marrow [24]. Fibrocytes circulate in the periphery and accumulate in tissues where injury occurs [25–28]. Fibrocytes have been extensively studied in lung fibrosis and skin wound healing, but not in cardiac remodeling processes [29–33].

In this study, we set to investigate whether all cardiac fibrob-lasts are able to produce GM-CSF or whether a specialized cardiac fibroblast subset is responsible for this pathogenic pathway that drives heart failure in both EAM and MI mouse models. We identified the main GM-CSF producers during cardiac inflammation to be a specific subset of cardiac fibroblasts, the stem cell antigen-1 positive (Sca-1^{+}) cardiac fibroblasts characterized by the

marker profile $CD45^{-}CD31^{-}CD29^{+}$mEF-$SK4^{+}PDGFR\alpha^{+}Sca\text{-}1^{+}$periostin^{+}. Specific ablation of IL-17A signaling to Sca-1^{+} cardiac fibroblasts protected mice from post-infarct heart failure and resulted mortality. Moreover, Sca-1^{+} cardiac fibroblasts exhibited plasticity and produced GM-CSF and CCL2 in response to a Th17 microenvironment, while they were able to be repolarized to secrete eotaxin when placed in a Th2 microenvironment. We also found a similar subset of GM-CSF-producing cardiac fibroblasts identified by the marker profile $CD45^{-}CD31^{-}CD29^{+}PDGFR\alpha^{+}$ in biopsies from heart failure patients of both myocarditis and ischemic origin. Thus, Sca-1^{+} cardiac fibroblasts are the specialized cardiac fibroblast subpopulation that produces GM-CSF and drives heart failure.

Results

Sca-1^{+} cardiac fibroblasts are potent GM-CSF-producers during cardiac inflammation

We described previously that cardiac fibroblasts produce GM-CSF in response to IL-17A during myocarditis [12]. To determine whether a specific cardiac fibroblast subset produces GM-CSF and the relative contribution to the overall cardiac GM-CSF production during myocarditis, we classified cardiac fibroblasts based on their surface marker expressions (Fig. 1A) [34]. The first subset was gated as $CD45^{-}CD31^{-}CD29^{+}$mEF-$SK4^{+}PDGFR\alpha^{+}Sca\text{-}1^{+}$ (depicted further as Sca-1^{+}) cardiac fibroblasts, and the second subset was gated as $CD45^{-}CD31^{-}CD29^{+}$mEF-$SK4^{+}$Sca-1^{-} (depicted as Sca-1^{-}) cardiac fibroblasts. As another possible source of cardiac fibroblasts during cardiac inflammation, fibrocytes were analyzed as the third subset and gated as $CD45^{+}CD31^{-}CD11b^{+}CD34^{+}CXCR4^{+}CollagenI^{+}$. All Sca-$1^{+}$ cardiac fibroblasts expressed the cardiac fibroblast marker, platelet-derived growth factor receptor alpha (PDGFRα), while cells expressing another fibroblast marker CD90 (as known as thymus cell antigen-1) were found in both Sca-1^{+} and Sca-1^{-} cardiac fibroblasts (Fig. 1A). We examined the numbers of cardiac fibroblast subsets in naïve hearts (day 0) and in the diseased hearts on days 14 and 21 of EAM (Fig. 1B). We observed a significant increase in the number of Sca-1^{+} cardiac fibroblasts on day 21 of EAM, but not on day 14 (Fig. 1B, C). In contrast, the number of Sca-1^{-} cardiac fibroblasts decreased on day 14 and remained diminished on day 21 (Fig. 1B, C). Very few fibrocytes were found in the naïve heart; the number of fibrocytes increased significantly on day 14 and continued to increase through day 21 of EAM (Fig. 1B, C).

We examined the GM-CSF production at day 21 of EAM and revealed that GM-CSF-positive cardiac fibroblasts were mostly Sca-1^{+} cardiac fibroblasts, while GM-CSF production by the other two cardiac fibroblast subsets was negligible (Fig. 1D). Using t-distributed stochastic neighbor embedding (t-SNE) clustering algorithm, we confirmed that most of GM-CSF-positive cardiac fibroblasts were in the cluster of Sca-1^{+} cardiac fibroblasts (Fig. 1E). To establish the relative contribution of Sca-1^{+} cardiac fibroblasts to the total GM-CSF production during EAM, we analyzed GM-CSF production by all cell types in the heart (Fig. 1F,G). Endothelial cells produced negligible amount of GM-CSF (Supporting Information Fig. 1A) and the number of endothelial cells was not changed during EAM development (Supporting Information Fig. 1B). On the other hand, the number of infiltrating leukocytes increased dramatically during EAM development (Supporting Information Fig. 1C), among which, lymphocytes and myeloid cells produced substantial

amounts of GM-CSF (Supporting Information Fig. 1A). However, the major GM-CSF producers were still Sca-1$^+$ cardiac fibroblasts among all GM-CSF-positive cardiac cells (Fig. 1F), and Sca-1$^+$ cardiac fibroblasts represented over 50% of GM-CSF-positive cardiac cells at day 21 of EAM (Fig. 1G). Thus, Sca-1$^+$ cardiac fibroblasts were not only active GM-CSF producers, but also the major source of GM-CSF during cardiac inflammation.

In order to determine whether the increase of GM-CSF-positive Sca-1$^+$ cardiac fibroblasts is specific to cardiac inflammation, we compared GM-CSF-positive Sca-1$^+$ cardiac fibroblasts from mice with EAM to that from mock-immunized mice (CFA alone) on day 21 post-immunization. Both the frequency and the number of GM-CSF-positive Sca-1$^+$ cardiac fibroblasts were significantly higher in EAM hearts compared to that in the hearts of the mock-immunized mice (Fig. 1H). In addition, both the frequency and the number of GM-CSF-positive Sca-1$^+$ cardiac fibroblasts were significantly lower in *Il17ra*$^{-/-}$ mice compared to that in the WT mice on day 21 of EAM (Fig. 1I). Therefore, GM-CSF production by Sca-1$^+$ cardiac fibroblasts is specific to cardiac inflammation and dependent on IL-17A signaling in EAM mouse model.

Sca-1$^+$ cardiac fibroblasts are potent cytokine producers and are plastic to environment changes

The dominant role of Sca-1$^+$ cardiac fibroblasts as the major GMCSF producers during EAM led us to investigate whether Sca-1$^+$ cardiac fibroblasts are capable of expressing other cytokines and chemokines during cardiac inflammation. We FACS-sorted Sca-1$^+$ and Sca-1$^-$ cardiac fibroblasts on day 21 of EAM and assessed the mRNA expression levels of various cytokines and chemokines. We detected significantly enriched mRNA expression levels of *Csf2, Ccl2, Cxcl10* and *Ccl11* in sorted Sca-1$^+$ cardiac fibroblasts compared to whole heart transcripts and sorted Sca-1$^-$ cardiac fibrob-lasts (Fig. 2A). In addition to the expression of these immune mediators in sorted Sca-1$^+$ cardiac fibroblasts, we detected significantly enriched mRNA expression levels of periostin (*Postn*) (Fig. 2A). Periostin is known to be upregulated in activated cardiac fibroblasts upon cardiac injury [34, 35].

Next, we isolated CD45$^-$CD31$^-$Sca-1$^+$ cardiac cells from na¨ıve adult mouse hearts and examined their responses to signature Th cytokines. Sca-1$^+$ cardiac fibroblasts expressed *Csf2* and *Ccl2* mRNA in response to IL-17A, while IL-13 and interferon gamma (IFN-γ) induced Sca-1$^+$ cardiac fibroblasts to express *Ccl11* and *Cxcl10* mRNA respectively (Fig. 2B). The ability of Sca-1$^+$ cardiac fibroblasts to express different cytokines in response to different signature Th cytokines led us to investigate whether Sca-1$^+$ cardiac fibroblasts exhibit plasticity, *i.e.* previously IL-17A-treated Sca-1$^+$ cardiac fibroblasts are capable to respond to signatureTh2 stimuli and start to produce eotaxin. To answer this question, we isolated Sca-1$^+$ cardiac fibroblasts from CCL2-mCherry reporter mice, these cells express mCherry following expression of CCL2 [36]. The majority of Sca-1$^+$ cardiac fibroblasts became mCherry-positive after culturing in the Th17 microenvironment (Fig. 2C). We used the combination of IL-17A and TNF-α as the representative Th17 microenvironment, as our lab and others have previously reported that TNF-α synergizes with IL-17A in the production of IL-17A-induced genes [12, 37]. After culturing CCL2-mCherry Sca-1$^+$ cardiac fibroblasts in the Th17 microenvironment for 3 days, we FACS-sorted mCherry-

positive cells on day 3 and re-cultured them in the Th2 microenvironment for another three days (Fig. 2D).

After three days of culture in the Th17 microenvironment, Sca-1$^+$ cardiac fibroblasts expressed *Ccl2* and *Csf2* mRNA, but not *Ccl11* mRNA (Fig. 2E). After FACS sorting and reculturing in Th2 microenvironment, we observed reduced levels of *Ccl2* and *Csf2* mRNA expression in the previous mCherry-positive cells, while *Ccl11* mRNA expression was upregulated (Fig. 2E). Protein levels of secreted CCL11 and GM-CSF in the culture supernatant followed the same trend (Fig. 2F). These results clearly demonstrated that Sca-1$^+$ cardiac fibroblasts are plastic and capable to be repolarized in response to changes in the microenvironments.

IL-17A induces GM-CSF production in Sca-1$^+$ cardiac fibroblasts through activation of NF-κB and NFAT2

Next, we investigated the signaling pathways that participate in the induction of GM-CSF production by Sca-1$^+$ cardiac fibrob-lasts. We performed phospho-flow cytometry on Sca-1$^+$ cardiac fibroblasts cultured in different Th microenvironments. It was previously reported in T lymphocytes, that synergistic activation of nuclear factor kappa-light-chain-enhancer of activated B cells (NF-κB) and Nuclear factor of activated T-cells 2 (NFAT2, as known as NFATc1) was observed during GM-CSF transcription activation [38, 39]. Few unstimulated Sca-1$^+$ cardiac fibroblasts were positive for phosphorylated p65 (RelA, component of NF-κB) (p-p65) and NFAT2, while about half of Sca-1$^+$ cardiac fibrob-lasts became p-p65$^+$NFAT2$^+$ under Th17 conditions (Fig. 3A). Moreover, GM-CSF was detected in most of these p-p65$^+$NFAT2$^+$ Sca-1$^+$ cardiac fibroblasts (Fig. 3A).

To further investigate the differences in signaling pathways under different Th conditions, we examined the protein levels and the phosphorylation state of various signaling molecules. We detected increased phosphorylation levels of p65, Signal transducer and activator of transcription 3 (Stat3) and Erk1/2 under both Th17 and Th2 conditions. Stat6 was only phosphorylated under Th2 conditions (Fig. 3B). We isolated the nuclear fraction from the stimulated cells and found that p65 nuclear translocation took place specifically under Th17 conditions (Fig. 3C), despite the fact that p65 was phosphorylated under both conditions (Fig. 3B). In contrast, Stat6 nuclear translocation only occurred under Th2 conditions (Fig. 3C). Thus, we revealed that Th17-induced GMCSF production by Sca-1$^+$ cardiac fibroblasts is associated with synergistic activation of NF-κB and NFAT2. The balance between NF-κB/NFAT2 and Stat6 activations determines the functional plasticity of Sca-1$^+$ cardiac fibroblasts during cardiac inflammation between Th17 and Th2 microenvironments.

IL-17A signaling ablation leads to less GM-CSF$^+$Sca-1$^+$ cardiac fibroblasts and reduced post-MI death

To test the pathological relevance of Sca-1$^+$ cardiac fibroblasts in ischemic heart failure development, we induced MI in mice via ligation of left anterior descending coronary artery. In line with our findings in the myocarditis model, Sca-1$^+$ cardiac fibroblasts produced GM-CSF and CCL2 2 days post-MI (Fig. 4A, B). A previous study showed that IL-17A ablation is protective in MI mouse model [11]. In our study, we found a similar protection from MI in

the IL-17A receptor (IL-17RA) knockout (*Il17ra*$^{-/-}$) mice (Fig. 4C, D). The survival rate of *Il17ra*$^{-/-}$ mice at day 28 post-MI was 88 %, compared to 50 % of WT mice (Fig. 4C). We also observed reduced infarct size in *Il17ra*$^{-/-}$ mice at day 28 post-MI (Fig. 4D, E). We found significantly fewer GM-CSF-positive Sca-1^{+} cardiac fibroblasts in *Il17ra*$^{-/-}$ mice compared to WT mice (Fig. 4F). Therefore, we showed the ablation of IL-17A signaling led to less GM-CSF-positive Sca-1^{+} cardiac fibroblasts, reduced infarct size and improved post-MI survival.

IL-17RA ablation in GM-CSF^{+}Sca-1^{+}Periostin^{+} cardiac fibroblasts attenuates post-MI heart failure

To test the requirement of IL-17A signaling specifically to GM-CSF-positive Sca-1^{+} cardiac fibroblasts in the development of post-MI heart failure and death, we searched for cardiac fibroblast specific Cre-expressing mice. Sca-1^{Cre} mice were not available to us; however, we found Sca-1^{+} cardiac fibroblasts expressed high levels of periostin (Fig. 2A). Periostin is a matrixcellular protein firstly identified in periosteum [40], but stands out as a specific marker for activated cardiac fibroblasts [41]. Moreover, we found that most GM-CSF-positive Sca-1^{+} cardiac fibroblasts were positive for periostin (GFP) in *Postn*$^{Cre/eGFP}$ reporter mice (Fig. 5A). Thus, we crossed *Il17ra*$^{fl/fl}$ mice to *Postn*$^{Cre/eGFP}$ mice to specifically ablate IL-17RA in periostin-positive cells (*Postn*^{Cre}*Il17ra*$^{fl/fl}$ mice). Specific ablation of IL-17RA in periostin^{+} cardiac fibroblasts limited the infarct region to a restricted area right below the occlusion site, whereas the infarct expanded to the whole left ventricles of the control mice (Fig. 5B). The infarct size of *Postn*^{Cre}*Il17ra*$^{fl/fl}$ mice (labeled as *Postn*$^{IL-17RAKO}$ in the figure) at day 7 post-MI was significantly smaller than that of the controls (Fig. 5C). The survival rate at day 28 post-MI was also improved by the specific ablation of IL-17RA in periostin^{+} cardiac fibroblasts (Fig. 5D). The number of GM-CSF^{+}Sca-1^{+} cardiac fibroblasts was significantly reduced in infarcted *Postn*^{Cre}*Il17ra*$^{fl/fl}$ hearts compared to control animals (Fig. 5E). In addition, we found that both the frequency and the number of Ly6C^{hi} inflammatory monocytes were significantly lower in the hearts of *Postn*^{Cre}*Il17ra*$^{fl/fl}$ mice compared to control mice (Fig. 5F, G, gating strategy for Ly6C^{hi} inflammatory monocytes illustrated in Supporting Information Fig. 2). We showed before that these Ly6C^{hi} inflammatory monocytes were correlated with cardiac fibrosis and heart failure development [12]. These results demonstrated that the ablation of IL-17A signaling to GM-CSF-expressing Sca-1^{+} (periostin^{+}) cardiac fibroblasts led to reduced GM-CSF production by Sca-1^{+} cardiac fibroblasts, decreased number of Ly6C^{hi} inflammatory monocytes, reduced infarct size and improved post-MI survival.

GM-CSF^{+} cardiac fibroblast subset in human's hearts exhibits similar functional plasticity

Next, we examined whether GM-CSF and other cytokines and chemokines are produced by a similar cardiac fibroblast subset in human cardiac fibroblasts, and whether these cardiac fibrob-lasts also exhibit similar functional plasticity. First, we acquired human primary cardiac fibroblasts isolated from the left ventricles of healthy donors from Cell Application, Inc. [42–44] and characterized them by flow cytometry. We detected three populations in these human cardiac fibroblasts based on CD29 and cKit expression, i.e. CD29^{+}cKit^{+}, CD29^{+}cKit^{-}, and CD29^{-}cKit^{-}cells (Fig. 6A). Using t-SNE clustering algorithm, we observed three automatically formed clusters (Fig. 6B), which matched the manually gated

populations (Fig. 6A). Mesenchymal stem cell markers, CD29, CD73 and CD105 were co-expressed by both $CD29^{+}cKit^{+}$ and $CD29^{+}cKit^{-}$ cells, while CD90 was expressed in $CD29^{+}cKit^{+}$ cells and some $CD29^{+}cKit^{-}$ cells. PDGFRα was expressed at intermediate levels by all three subsets, while cKit and another cardiac fibroblast marker, discoidin domain receptor 2 (DDR2), were co-expressed only in $CD29^{+}cKit^{+}$ cells. GM-CSF was expressed by $CD29^{+}cKit^{+}$ and $CD29^{+}cKit^{-}$ cells, but not $CD29^{-}cKit^{-}$ cells (Fig. 6C). Further analysis on the cytokine expression profiles of these human cardiac fibroblasts revealed that IL-17A induced the mRNA expression of *CCL2* and *CSF2*, whereas increased mRNA expression levels of eotaxins *CCL11, CCL24* and *CCL26* was detected after IL-13 stimulation (Fig. 6D). When Th microenvironments were changed from Th17 to Th2 conditions, we detected reduced *CSF2* mRNA expression, while *CCL11*, *CCL24* and *CCL26* mRNA expression levels were upregulated (Fig. 6E). The protein concentration of secreted GM-CSF and CCL11 in the culture supernatant followed the same trend (Supporting Information Fig. 3). Therefore, human GM-CSF-expressing cardiac fibroblasts, identified by markers CD29, PDGFRα, CD73 and CD105, exhibit similar functional plasticity to be repolarized as mice GM-CSF-expressing cardiac fibroblasts.

Human cardiac fibroblasts from heart failure patients produce GM-CSF and CCL2

To confirm the data from human cardiac fibroblast in vitro culture, we examined biopsy samples from patients with myocarditis and ischemic cardiomyopathy undergoing implantation of left ventricular assist devices. Using flow cytometry, we identified the cardiac fibroblasts in these biopsy samples as $CD45^{-}CD31^{-}CD29^{+}PDGFR\alpha^{+}$ (Sca-1 is not expressed in humans) cells (Fig. 7A). These $PDGFR\alpha^{+}$ cardiac cells expressed the same set of mesenchymal cell markers, including CD29 and PDGFRα, similar to the $Sca\text{-}1^{+}$ ($PDGFR\alpha^{+}$) cardiac fibroblasts we have described in mice and the in vitro cultured human cardiac fibroblasts. Moreover, we showed that $PDGFR\alpha^{+}$ cells were source of GM-CSF or CCL2, whereas $PDGFR\alpha^{-}$ cells were negative for GM-CSF and CCL2 staining (Fig. 7A). We observed strong GM-CSF production in human $PDGFR\alpha^{+}$ cardiac fibroblasts from myocarditis patients (Fig. 7B). CCL2 was identified only in one patient (Fig. 7B). In contrast, in biopsies from ischemic patients, we observed CCL2-positive $PDGFR\alpha^{+}$ cardiac fibroblasts in three out of five patients, and GM-CSF-positive $PDGFR\alpha^{+}$ cardiac fibroblasts were found in four out of five patients (Fig. 7C). All cardiac samples evaluated by flow cytometry were acquired when left ventricular assist device was implanted due to severe heart failure. The histology evaluation of the samples reviled advanced fibrotic changes with ongoing inflammation (Supporting Information Fig.4). Thus, we identified GM-CSF- and CCL2-exprssing $PDGFR\alpha^{+}$ cardiac fibroblasts in both myocarditis and ischemic heart failure patients, however, the finding was not consistent for all ischemic patients.

Discussion

For decades cardiac fibroblasts were mostly known as extracellular matrix protein producers [45, 46]. We identified a specific cardiac fibroblast subset that drives the development of heart failure as potent producers of inflammatory cytokines and chemokines. This cardiac fibroblast subset, defined as $CD45^{-}CD31^{-}CD29^{+}$mEF $SK4^{+}PDGFR\alpha^{+}Sca\text{-}1^{+}periostin^{+}$ ($Sca\text{-}1^{+}$) cardiac fibroblasts, are capable of producing various cytokines and chemokines,

such as GM-CSF and CCL2 during the progression of cardiac disease from inflammation to heart failure. The number of Sca-1$^+$ cardiac fibroblasts increased dramatically in both myocarditis and MI mouse models, and the GM-CSF-expressing Sca-1$^+$ cardiac fibroblasts represented over 50% of total GM-CSF-expressing cells in the diseased hearts. The GM-CSF production by cardiac fibroblasts was first shown by us in the EAM mouse model [12], and later by another two groups in Kawasaki disease and MI models [13, 14]. However, it remained elusive whether all cardiac fibroblasts are responsible for the production of GM-CSF. Here we further characterized the heterogeneous cardiac fibroblast population and found GM-CSF production only in Sca-1$^+$ cardiac fibroblasts among all cardiac resident cells. Moreover, we established that the production of GM-CSF by Sca-1$^+$ cardiac fibroblasts is a general mechanism for multiple cardiac diseases, including myocarditis and myocardial infarction.

In addition to GM-CSF, Sca-1$^+$ cardiac fibroblasts also produce other cytokines and chemokines, including CCL2, CXCL10 and eotaxin during cardiac inflammation. The capability of Sca-1$^+$ cardiac fibroblasts to produce different cytokines and chemokines revealed the complexity of the local cytokine microenvironments in cardiac inflammation. Ablating IL-17A or IL-4 protected mice from the development of DCMi, while removing IFN-γ or IL-13 led to more severe diseases in the EAM mouse model [10, 12, 47–50]. Thus, maintaining the right balance among different Th-directed cytokines is critical in preventing or limiting the progression of cardiac diseases to heart failure. We recently reported in a model of eosinophilic myocarditis that cardiac fibroblasts are potent producers of eotaxin 1 (CCL11), which is the main chemokine that regulates eosinophil trafficking to the heart [51]. In this study, we used the Sca-1$^+$ cardiac fibroblasts from CCL2-mCherry reporter mice to demonstrate that the previous GM-CSF- and CCL2-expressing Sca-1$^+$ cardiac fibroblasts are capable of switching to CCL11 producers after repolarization from Th17 to Th2 conditions. Moreover, we demonstrated here that conditional knockout mice that cannot receive IL-17A signaling to periostin-expressing cardiac fibroblasts, that are mostly GM-CSF-producing Sca-1$^+$ cardiac fibroblasts, have reduced frequency and number of inflammatory Ly6C^{hi} monocytes infiltrating the hearts. Sca-1$^+$ cardiac fibroblasts thus have a decisive role in what immune cells will traffic to the heart and by affecting myeloid populations these cells drive heart failure development. Therefore, Sca-1$^+$ cardiac fibroblasts are potential therapeutic targets to manipulate the balance of local cytokines and chemokines to manipulate the recruitment of immune cells during the inflammatory phase of myocarditis or myocardial infarction.

The induction of GM-CSF production in T cells involves the activation of both NF-κB and NFAT2 [38, 39, 52–57]. The activation of NF-κB pathway was also reported in TNF-α- and IL-17A-induced activation of synovial fibroblasts and endothelial cells [58, 59]. In our study, we revealed that the same synergistic activation of NF-κB and NFAT2 promoted IL-17A-induced GM-CSF production in Sca-1$^+$ cardiac fibroblasts. However, we did not detect the activation of p38 mitogen-activated protein kinase (MAPK) pathway that was previously reported in TNF-α-induced GM-CSF production [60]. We also found Stat6 activation directed the signaling pathways in Th2 conditions. These results suggest that the balance between NF-κB/NFAT2 and Stat6 activations determine the functional plasticity of

Sca-1$^+$ cardiac fibroblasts and manipulating the activation balance in Sca-1$^+$ cardiac fibroblasts could be a potential therapeutic strategy.

In the MI model, both IL-17A [11] and GM-CSF [61] were shown to be pathogenic and promote the development of heart failure. GM-CSF was also recently reported to act locally and distally after onset of MI to generate and recruit inflammatory cells [14]. We connected the two pathogenic factors, IL-17A and GMCSF, through the Sca-1$^+$ cardiac fibroblast subset, which responds to IL-17A to produce GM-CSF. We detected significantly fewer GMCSF-positive Sca-1$^+$ cardiac fibroblasts in infarcted *Il17ra*$^{-/-}$ mice compared to infarcted WT mice. The reduction in the number of GM-CSF-positive Sca-1$^+$ cardiac fibroblasts also correlates to the reduction of infarct size and improvement of post-MI survival rate of infarcted *Il17ra*$^{-/-}$ mice.

The co-expression of periostin, a marker of activated cardiac fibroblasts [34, 41], by most GM-CSF-positive Sca-1$^+$ cardiac fibroblasts enabled us to specifically ablate IL-17A signaling to GM-CSF-expressing Sca-1$^+$ cardiac fibroblasts through *Postn*^{Cre}*Il17ra*$^{fl/fl}$ mice. The specific deletion of IL-17RA in periostin$^+$ cardiac fibroblasts resulted in reduced number of GM-CSF-positive Sca-1$^+$ cardiac fibroblasts and this reduction correlates with smaller infarct size and improved post-MI survival rate. It has been recently reported that the ablation of periostin$^+$ cardiac fibroblasts prevents adverse cardiac remodeling after MI [62], however, the mechanism behind the cardiac remodeling driven by periostin$^+$ cardiac fibroblasts was not stated. Based on our results we speculate that the mechanism could have been the deletion of GM-CSF-expressing cardiac fibroblasts since we demonstrated that the pathological GM-CSF-expressing Sca-1$^+$ cardiac fibroblasts are periostin-positive.

To confirm our findings in mice, we examined both in vitro cultured human primary cardiac fibroblasts and human heart failure patient endomyocardial biopsy samples for similar GM-CSF-expressing cardiac fibroblast subset. We characterized the human primary cardiac fibroblasts and found similar GM-CSF-expressing cardiac fibroblasts that express human mesenchymal stem cell markers, including CD29, CD73 and CD105 [63–65]. These cardiac fibroblasts are potent cytokine producers and exhibit similar functional plasticity in response to different microenvironments similar to the mouse Sca-1$^+$ cardiac fibroblasts. Moreover, GM-CSF- and CCL2-expressing cardiac fibroblasts were also found in the cardiac biopsy samples from myocarditis and ischemic heart failure patients. In endomyocardial biopsies from myocarditis patients, most PDGFRα$^+$ cells expressed GM-CSF. However, in endomyocardial biopsy samples from ischemic heart failure patients, PDGFRα$^+$ cells were mostly positive for CCL2, whereas, GM-CSF staining pattern was not consistent. The patients in our cohort were biopsied when they received left ventricular assist device for severe heart failure. Some patients were acute, like myocarditis patient number four, who had giant cell myocarditis and died a few days later. This patient had pronounced production of GM-CSF and CCL2 by PDGFRα$^+$ cardiac fibroblasts and quite a substantial amount of ongoing inflammation was observed together with ongoing fibrosis. Most other patients were chronic with histological changes indicating fibrosis with ongoing mild to moderate inflammation in the heart. Further study is needed to make a conclusion on the role of fibroblasts secreting GM-CSF and CCL-2 in the pathogenesis of human myocarditis and ischemic cardiomyopathy.

The Sca-1$^+$ cardiac fibroblasts we identified here might overlap with previously described Sca-1$^+$ cardiac progenitor cells in previous mouse studies, as they share common markers including CD29, Sca-1 and PDGFRα [34, 66–69]. Although Sca-1 is not expressed in humans, we found the human GM-CSF-expressing cardiac fibroblasts were positive for PDGFRα and also multiple mesenchymal stem cell markers that were described previously, including cKit, CD29, CD73 and CD105 [63–65]. The expression of CD29, CD73 and CD105 indicates their mesenchymal origin and c-Kit marked their stem cell like properties and potential to differentiate to other cell types [63]. The cytokine repolarization experiments with primary human cardiac fibroblasts suggested that, just like the mouse Sca-1$^+$ cardiac fibroblasts, these human cardiac fibroblasts are also plastic and able to repolarize based on the changes in their microenvironment.

Materials and methods

Patients

We obtained endomyocardial biopsy samples from the apex of the left ventricle of patients with advanced heart failure undergoing implantation of left ventricular assist devices at the Texas Heart Institute. Informed consent was obtained from human subjects and the study protocol was approved by the Committee for the Protection of Human Subjects (University of Texas Health Science Centre at Houston. IRB # HSC-MS-05–0074) as previously described [70]. Heart samples were preserved frozen in liquid nitrogen (−196°C) and kept at −80°C in the tissue bank at the Texas Heart Institute, Houston, TX. Patient's information of all samples was processed with random non-linked code relabeling in a database at the time of preservation. Aliquots of the samples were shipped frozen and processed in our lab for flow cytometry.

Mice

WT BALB/cJ mice (6–10 weeks old, JAX000651) and WT C57BL/6J mice (8–12 weeks old, JAX000664), *Ccl2*$^{fl/fl}$-mCherry (*Ccl2*-RFP^{flox}, JAX016849) [36] mice were purchased from the Jackson Laboratories (Bar Harbor ME). *Il17ra*$^{-/-}$ mice [71] on the BALB/c background were provided by Amgen Inc. (Thousand Oaks, CA) and Dr. J. Kolls (Children's Hospital, University of Pittsburgh Medical Center, Pittsburgh, PA). *Il17ra*$^{fl/fl}$ mice [72] were provided on the C57BL/6 background by Dr. Ari Waisman (Institute für Molekulare Medizin Mainz, Germany) and *Postn*$^{Cre/eGFP}$ mice [73] were provided on the C57BL/6 background by Dr. Simon Conway (Indiana University School of Medicine, Indianapolis, IN). Mice used for EAM model in this study were on the BALB/c background and mice used for MI model were on either the BALB/c background (*Il17ra*$^{-/-}$ mice) or the C57BL/6 background (*Il17ra*$^{fl/fl}$ mice and *Postn*$^{Cre/eGFP}$ mice). Mice were housed in specific pathogen–free animal facilities at the Johns Hopkins University. Experiments were conducted on 6–10-wk-old age-matched male mice (EAM) or 8–16-wk-old age-matched male mice (MI) in compliance with the Animal Welfare Act and the principles set forth in the Guide for the Care and Use of Laboratory Animals. All methods and protocols were approved by the Animal Care and Use Committee of Johns Hopkins University.

EAM mouse model

To induce EAM, mice on BALB/c background received subcutaneous immunizations on days 0 and 7 of 125 μg per mouse of myosin heavy chain α peptide ($MyHC\alpha_{614–629}$) (AcSLKLMATLFSTYASAD; commercially synthesized by fMOC chemistry and purified to a minimum of 90 % by HPLC, Genscript) [74] emulsified in CFA (Sigma-Aldrich) supplemented to 5 mg/mL heat-killed Mycobacterium tuberculosis strain H37Ra (Difco). On day 0, mice also received 500 ng pertussis toxins intraperitoneally (List Biologicals) [75]. Mouse hearts were harvested on days 0, 14 or 21 for flow cytometry analysis.

MI mouse model

To induce MI, mice were subjected to permanent ligation of the left anterior descending coronary artery or to a sham operation without ligation [76]. Briefly, mice were anesthetized with 3.5 % isoflurane (Baxter), endotracheally intubated, and mechanically ventilated with 1.5 % isoflurane (Baxter) throughout the operation process via small animal ventilator (Model 845, Harvard Apparatus). Pre-operational analgesics (0.05 mg/kg Buprenorphine, Reckitt Benckiser) and paralytics (1 mg/kg Succinylcholine, Henry Schein) were administered prior to operation. Mice were subjected to thoracotomy typically around the 3rd or 4th intercostal space. An 8–0 polyethylene suture was advanced sub-epicardially and perpendicular to the left anterior descending coronary artery. For permanent occlusion, a ligature was tightened around the artery, and could be visualized by myocardial bleaching and loss of motion below the occlusion. The chest and skin were closed with a 6–0 nylon suture followed by removal of air from the thorax via a pleural catheter. The procedure was performed by the same surgeon blinded to genotypes. Mice that died during recovery from anesthesia were excluded. Sham-operated animals underwent the same procedure without coronary artery ligation. Mice were sacrificed, and hearts were harvested on days 2 or 4 post-MI for flow cytometry analysis, or on days 7 or 28 post-MI to assess cardiac remodeling outcomes.

Infarct size evaluation

Heart tissues were fixed in SafeFix solution (Thermo-Fisher Scientific), embedded in paraffin, and cut into 5-μm-thick sections. Hematoxylin and eosin (H&E) and Masson's trichrome staining (HistoServ) were performed on paraffin-embedded sections to determine the infarct size. Three sections were used to calculate the infarct size, *i.e.* a section right below the ligation site (Section A), a section near the apex (Section C) and Section B at a midpoint of sections A and C. The infarct size was calculated as the total infarct circumference of all three sections divided by the total left ventricle circumference of all three sections [77].

Processing human cardiac samples

Sample weights ranged between 80 mg and 300 mg. Specimens were cut into fragments of approximately 2 mm^3. Fragments were placed in GentleMACS C Tubes (Miltenyi Biotec) in 5 mL of enzymatic digestion buffer composed of 5 mL of Hank's Balanced Salt Solution [HBSS] (Corning) with 600 U/mL of Collagenase II and 60 U/mL of DNase I (Worthington Biochemical Corporation) and mechanically dissociated with GentleMACS (Miltenyi

Biotec). Samples were digested for 30 min at 37°C with shaking, and mechanically dissociated with GentleMACS (Miltenyi Biotec) again. Cell suspensions were filtered through 40 μm cell strainers (Bioland Scientific). Finally, cells were washed and resuspended in PBS with cell concentration adjusted to 10^6–10^7 cells/200 μL of PBS for antibody staining.

Processing mouse cardiac cells

Mouse cardiac cells were isolated by perfusing the mouse hearts for 3 min with PBS and digested in GentleMACS C Tubes (Miltenyi Biotec) with 5 mL of enzymatic digestion buffer composed of 5 mL HBSS (Corning) supplemented with 3,000 U/mL Collagenase II and 90 U/mL DNase I (Worthington Biochemical Corporation). Samples were digested for 30 min at 37°C with shaking. Mechanical dissociation with GentleMACS (Miltenyi Biotec) was performed before and after the 30-minute incubation [78]. Cells were filtered through a 40 μm cell strainer (Bioland Scientific), washed and resuspended in PBS. For intracellular cytokine staining, cells were stimulated in vitro for 4 h with 50 ng/mL Phorbol 12-myristate 13-acetate (PMA), 750 ng/mL ionomycin (Sigma-Aldrich), Golgi Stop, and Golgi Plug (BD) before staining. Cells were washed in PBS prior to antibody staining. For isolation of primary adult mouse Sca-1^+ cardiac fibroblasts, processed cardiac cells were subjected to Histopaque1119 gradient (Sigma-Aldrich) to remove dead cells and debris according to the manufacturer's instructions. Leukocytes and endothelial cells were removed by CD45 and CD31 MACS paramagnetic depletion (Miltenyi Biotec) and Sca-1^+ cells were isolated using Sca-1 MACS paramagnetic positive selection following manufacturer's instructions. Cells were washed and seeded on culture flasks.

Processing mouse splenocytes

Single-cell suspension of splenocytes was made from the mouse spleen by mechanical dissociation followed by the lysis of red blood cells with ACK lysis buffer (Quality Biologicals), filtered through a 70 μm cell strainer (Bioland Scientific), washed and resuspended in PBS. Splenocytes were used for compensation controls for flow cytometry analysis.

Human primary cardiac fibroblasts

We acquired human primary cardiac fibroblasts from Cell Applications, Inc (San Diego, CA). Cells were thawed at 37°C immediately after taken out from liquid nitrogen (−196°C), washed and seeded on uncoated culture flasks in human cardiac fibrob-lasts growth medium according to manufacturer's instructions (Cell Applications). Cells were passaged every 2–3 days. For stimulation, cells were seeded on 6-well plates and stimulated with 50 ng/mL of recombinant human IL-17A (Peprotech) for the Th17 conditions or 100 ng/mL of recombinant human IL-13 (Peprotech) for the Th2 conditions for three days. For flow cytometry, cells were detached using 0.05% trypsin-EDTA (Quality Biologicals) and washed in PBS prior to antibody staining. For cytokine repolarization experiments, cell culture supernatant was harvested, and cells were washed with PBS and cultured for another three days with new stimuli according to experiment design. Unstimulated cells were used as controls. Supernatant was collected upon harvest and stored at −80°C. Secreted cytokine levels were measured by quantitative sandwich ELISA.

Mouse primary Sca-1$^+$ cardiac fibroblasts

Sca-1$^+$ cardiac cells were isolated using MACS sorting beads as described above, and then seeded on culture flasks (Corning) in adult mouse cardiac fibroblast culture medium (DMEM with 4.5 g/L glucose, 2 mM L-glutamine, 1 mM sodium pyruvate, 25 mM Hepes, 100 U/mL penicillin G, 100 μg/mL streptomycin, 250 ng/mL amphotericin B, and 20 % FBS). Cells were passaged every 3–4 days. For stimulation, cells were seeded on 24-well plates and stimulated with 50 ng/mL of recombinant mouse IL-17A, 100 ng/mL of recombinant mouse IL-13, 50 ng/mL of recombinant mouse IFN-γ, 20 ng/mL of recombinant mouse TNF-α, or combinations of two cytokines for three days based on the experiment designs. All recombinant mouse cytokines were purchased from Peprotech (Rocky Hill, NJ). For flow cytometry, cells were detached using 0.05% trypsin-EDTA (Quality Biologicals) and washed in PBS prior to antibody staining. For cytokine repolarization experiments, cell culture super-natant was harvested, and cells were washed with PBS and cultured for another three days with new stimuli according to the experiment designs. Unstimulated cells were used as controls. Supernatant was collected upon harvest and stored at −80°C. Secreted cytokine levels were measured by quantitative sandwich ELISA.

Flow cytometry and fluorescence activated cell sorting (FACS)

Cell viability was determined by LIVE/DEAD staining according to the manufacturer's instructions (Life Technologies). Prior to surface immunostaining, samples were incubated with unconjugated Fc Receptor Binding Inhibitor (eBioscience). Cell surface markers were then stained with antibodies conjugated with fluorochromes (eBiosciences, BD and BioLegend). For intracellular cytokine staining, cells were fixed in CytoFix/CytoPerm (BD) and stained with antibodies against cytokines in Perm/Wash Buffer (BD). For phosphor flow of signaling molecules, cells were fixed in CytoFix/CytoPerm (BD) and stained with antibodies against signaling molecules in BD PhosFlow Perm/Wash Buffer (BD). Samples were acquired on the LSR II or LSR Fortessa cytometer running FACS Diva 6 (BD). For FACS isolation, single cell suspension from mouse hearts was further purified with a Histopaque-1119 gradient separation (Sigma-Aldrich) to eliminate dead cells and debris. Cells were then stained with antibodies conjugated with fluorochromes (eBioscience, BD, and BioLegend) and sorted with FACSAria Ilu Cell Sorter (BD). Antibodies used are listed in Supporting Information Table 1. Data were analyzed with Flow Jo 10.4 (Tree Star) and the t-distributed stochastic neighbor-embedding (t-SNE) algorithm embedded in FlowJo 10.4.

Immunoblot

We carried out immunoblot assays as previously described [79]. In brief, we cultured mouse primary Sca-1$^+$ cardiac fibroblasts under the Th17 conditions (50 ng/mL of IL-17A and 20 ng/mL TNF-α) or the Th2 conditions (100 ng/mL of IL-13) for the duration indicated, harvested, and lysed on ice by lysis buffer (50 mM Tris-HCl [pH 8.0], 150 mM NaCl, 1 % NP-40 and 0.5 % sodium deoxy cholate, 1x complete protease inhibitor cocktail (Roche Applied Science) for 30 min. Subcellular fractionation was performed by differential centrifugation as previously described [80]. The lysates or nuclear fractions were centrifuged

at 10 000× *g* at 4°C for 10 min, and the supernatant was separated by SDS-PAGE under reducing and denaturing conditions. The resolved protein bands were transferred onto nitrocellulose membranes and probed by the Super Signaling system (Thermo-Fisher Scientific) according to the manufacturer's instructions and imaged using FluorChem E System (Protein Simple). Antibodies used are listed in Supporting Information Table 1.

ELISA

Supernatant collected from cell culture was stored at −80°C before analysis. Protein levels of secreted GM-CSF and CCL11 were determined by quantitative sandwich ELISA according to manufacturer's recommended protocols (R&D Systems).

Quantitative PCR

Total RNA from cardiac tissues, FACS isolated cells or cultured cells was extracted in TRIzol (Invitrogen) and quantitated. Single-stranded cDNA was synthesized with the High Capacity cDNA Reverse Transcription kit (Thermo-Fisher Scientific). Expression levels of mouse genes were detected using quantitative real-time PCR with iQ SYBR Green Master mix (Bio-Rad Laboratories) and acquired on the MyiQ2 thermocycler with iQ5 software (Bio-Rad Laboratories). Quantitative real-time TaqMan PCR was performed for human genes and acquired on the MyiQ2 thermocycler with iQ5 software (Bio-Rad Laboratories). Data were analyzed by the $2^{-\mathrm{Ct}}$ method [81], normalizing threshold cycles first to *Gapdh* (for mouse gene analysis) or *HPRT1* (for human gene analysis) expression and then to biological controls. The following TaqMan primers for human genes (Applied Biosystems) were used: *CSF2* (Hs00929873 m1), *CCL2* (Hs00234140 m1), *CCL11* (Hs00237013 m1), *CCL24* (Hs00171082 m1), *CCL26* (Hs00171146 m1) and the housekeeping gene *HPRT1* (Hs02800695 m1). Mouse primers used are listed in Supporting Information Table 2.

Statistics

Two groups with normally distributed data were analyzed using Student's *t*-test. Mann-Whitney test was used to analyze discontinuous parametric data. Multiple group analysis was performed by one-way ANOVA followed by Tukey's multiple comparisons test for continuous variables. Survival analysis was performed by the Kaplan-Meier method and compared by Log-rank (Mantel-Cox) test. Calculations were performed in Prism 6 (Graph Pad Software). *P*-values of 0.05 or less were considered statistically significant and are denoted by asterisks: $^{*}p < 0.05$; $^{**}p < 0.01$; $^{***}p < 0.001$.

Study approval

Human study protocol was approved by the Committee for the Protection of Human Subjects at University of Texas Health Science Centre at Houston with IRB # HSC-MS-05–0074. All animal studies were performed with the approval of the Institutional Animal Care and Use Committee at Johns Hopkins University School of Medicine. These investigations followed the Guide for the Care and Use of Laboratory Animals, published by the National Institutes of Health.

Supplementary Material

Refer to Web version on PubMed Central for supplementary material.

Acknowledgements:

This work was supported by grants from NIH/NHLBI (R01HL118183 and R01HL136586) to Daniela Čiháková, American Heart Association AWRP Winter 2017 Grant-in-Aid (17GRNT33700274) to Daniela Čiháková Matthew Poyner MVP Memorial Myocarditis Research Fund to Daniela Čiháková and Nisha Gilotra, Myocarditis Foundation Postdoctoral Fellowship (90072351) to Guobao Chen, American Heart Association Postdoctoral Fellowship (16POST31330012) to William Bracamonte-Baran, the Richard J. and Margaret Conn Himelfarb Student Support Fund, Johns Hopkins Autoimmune Disease Research Center O'Leary-Wilson Fellowship and Johns Hopkins Bloomberg School of Public Health Katherine E. Welsh Fellowship to Xuezhou Hou. This work was also supported in part by NIH grants to Simon J. Conway (R01 HL135657), Heinrich Taegt-meyer (R01 HL6148315) and NIH/NIGMS grant (R01GM111682) to Fengyi Wan. We are also grateful to Amgen Inc. (Thousand Oaks, CA) and Dr. J. Kolls (Children's Hospital, University of Pittsburgh Medical Center, Pittsburgh, PA) for *Il17ra*$^{-/-}$ mice; MichelleK. Leppo (Missy) (Cardiovascular Physiology and Surgery Core) for teaching Guobao Chen the MI mouse survival surgery; Xiaoling Zhang (JHMI Ross Flow Cytometry Core) and Hao Zhang (JHU SPH FACS Sorting Core) for cell sorting; Julie Schaub for mouse colony management; Jobert G. Barin, David Hughes and Jarrett Venezia for proofreading.

Abbreviations:

CCL11	C-C motif chemokine ligand 11 (eotaxin 1)
CCL2	C-C motif chemokine ligand 2
CCL24	C-C motif chemokine ligand 24 (eotaxin 2)
CCL26	C-C motif chemokine ligand 26 (eotaxin 3)
CF	Cardiac fibroblast
Csf2	GM-CSF gene name
CXCL10	C-X-C motif chemokine ligand 10
DCMi	Inflammatory dilated cardiomyopathy
DDR2	Discoidin domain receptor 2
EAM	Experimental autoimmune myocarditis
Erk1/2	Extracellular signal-regulated kinase 1/2
GM-CSF	Granulocyte macrophage colony-stimulating factor
IFN-γ	Interferon gamma
IL-13	Interleukin 13
IL-17A	Interleukin 17A
IL17RA	IL-17A receptor A
MAPK	Mitogen-activated protein kinase
MI	Myocardial infarction

NFAT2	Nuclear factor of activated T-cells 2
NF-κB	Nuclear factor kappa-light-chain-enhancer of activated B cells
PDGFRα	Platelet-derived growth factor receptor alpha (CD140α)
PMA	Phorbol 12-myristate 13-acetate
Postn	Periostin gene name
Sca-1	Stem cell antigen-1
Stat3	Signal transducer and activator of transcription 3
Stat6	Signal transducer and activator of transcription 6
Th17	T helper type 17
Th2	T helper type 2
TNF-α	Tumor necrosis factor alpha
t-SNE	t-distributed stochastic neighbor embedding
WT	Wild type

References

1. Benjamin EJ, Blaha MJ, Chiuve SE, Cushman M, Das SR, Deo R, de Ferranti SD et al., Heart Disease and Stroke Statistics-2017 Update: a report from the American Heart Association. Circulation 2017 135: e146–e603. [PubMed: 28122885]
2. Giamouzis G, Kalogeropoulos A, Georgiopoulou V, Laskar S, Smith AL, Dunbar S, Triposkiadis F et al., Hospitalization epidemic in patients with heart failure: risk factors, risk prediction, knowledge gaps, and future directions. J. Card. Fail 2011 17: 54–75. [PubMed: 21187265]
3. Roger VL, Epidemiology of heart failure. Circ. Res 2013 113: 646–659. [PubMed: 23989710]
4. Braunwald E, Heart failure. JACC Heart Fail 2013 1: 1–20. [PubMed: 24621794]
5. Bloom MW, Greenberg B, Jaarsma T, Januzzi JL, Lam CSP, Maggioni AP, Trochu J-N et al., Heart failure with reduced ejection fraction. Nat. Rev. Dis. Primers 2017 3: 17058. [PubMed: 28836616]
6. Chavey WE, Hogikyan RV, Van Harrison R **and** Nicklas JM, Heart failure due to reduced ejection fraction: medical management. Am. Fam. Physician 2017 95: 13–20. [PubMed: 28075105] **and**
7. Cooper LT, Myocarditis. N. Engl. J. Med 2009 360: 1526–1538. [PubMed: 19357408]
8. Dimas Van., Denfield SW, Friedman RA, Cannon BC, Kim JJ, Smith E.O'.Brian., Clunie SK et al., Frequency of cardiac death in children with idiopathic dilated cardiomyopathy. Am. J. Cardiol 2009 104: 1574–1577. [PubMed: 19932795]
9. Pietra BA, Kantor PF, Bartlett HL, Chin C, Canter CE, Larsen RL, Edens RE et al., Early predictors of survival to and after heart transplantation in children with dilated cardiomyopathy. Circulation 2012 126: 1079–1086. [PubMed: 22800850]
10. Baldeviano GC, Barin JG, Talor MV, Srinivasan S, Bedja D, Zheng D, Gabrielson K et al., Interleukin-17A is dispensable for myocarditis but essential for the progression to dilated cardiomyopathy. Circulation Res. 2010 106: 1646–1655. [PubMed: 20378858]
11. Yan X, Shichita T, Katsumata Y, Matsuhashi T, Ito H, Ito K, Anzai A et al., Deleterious effect of the IL-23/IL-17A axis and gammadeltaT cells on left ventricular remodeling after myocardial infarction. J. Am. Heart Assoc 2012 1: e004408. [PubMed: 23316306]
12. Wu L, Ong S, Talor MV, Barin JG, Baldeviano Gan., Kass DA, Bedja D et al., Cardiac fibroblasts mediate IL-17A-driven inflammatory dilated cardiomyopathy. J. Exp. Med 2014 211: 1441–1456.

13. Stock AT, Hansen JA, Sleeman MA, McKenzie BS **and** Wicks IP, GM-CSF primes cardiac inflammation in a mouse model of Kawasaki disease. J. Exp. Med 2016.**and**

14. Anzai A, Choi JL, He S, Fenn AM, Nairz M, Rattik S, McAlpine CS et al., The infarcted myocardium solicits GM-CSF for the detrimental oversupply of inflammatory leukocytes. J. Exp. Med 2017 214: 3293–3310. [PubMed: 28978634]

15. Deb A **and** Ubil E, Cardiac fibroblast in development and wound healing. J. Mol. Cell. Cardiol 2014 70: 47–55. [PubMed: 24625635]

16. Fries KM, Blieden T, Looney RJ, Sempowski GD, Silvera MR, Willis RA **and** Phipps RP, Evidence of fibroblast heterogeneity and the role of fibroblast subpopulations in fibrosis. Clin. Immunol. Immunopathol 1994 72: 283–292. [PubMed: 7914840] **and**

17. Lajiness JD **and** Conway SJ, Origin, development, and differentiation of cardiac fibroblasts. J. Mol. Cell. Cardiol 2014 70: 2–8. [PubMed: 24231799]

18. Lie-Venema H, van den Akker NMS, Bax NAM, Winter EM, Maas S, Kekarainen T, Hoeben RC et al., Origin, fate, and function of epicardium-derived cells (EPDCs) in normal and abnormal cardiac development. Scientific World Journal 2007 7: 1777–1798. [PubMed: 18040540]

19. von Gise A **and** Pu WT, Endocardial and epicardial epithelial to mesenchymal transitions in heart development and disease. Circ. Res 2012 110: 1628–1645. [PubMed: 22679138]

20. Smart N, Dubé KN **and** Riley PR, Epicardial progenitor cells in cardiac regeneration and neovascularisation. Vascul. Pharmacol 2013 58: 164–173. [PubMed: 22902355] **and**

21. Chong JJH, Chandrakanthan V, Xaymardan M, Asli NS, Li J, Ahmed I, Heffernan C et al., Adult cardiac-resident MSC-like stem cells with a proepicardial origin. Cell Stem Cell 2011 9: 527–540. [PubMed: 22136928]

22. Paylor B, Fernandes J, McManus B **and** Rossi F, Tissue-resident Sca1^{+} PDGFRalpha^{+} mesenchymal progenitors are the cellular source of fibrofatty infiltration in arrhythmogenic cardiomyopathy. F1000Res 2013 2: 141. [PubMed: 24358871] **and**

23. Bollini S, Vieira JMN, Howard S, Dubé KN, Balmer GM, Smart N **and** Riley PR, Re-activated adult epicardial progenitor cells are a heterogeneous population molecularly distinct from their embryonic counterparts. Stem Cells Dev. 2014 23: 1719–1730. [PubMed: 24702282] **and**

24. Bucala R, Spiegel LA, Chesney J, Hogan M **and** Cerami A, Circulating fibrocytes define a new leukocyte subpopulation that mediates tissue repair. Mol. Med 1994 1: 71–81. [PubMed: 8790603] **and**

25. Phillips RJ, Burdick MD, Hong K, Lutz MA, Murray LA, Xue YY, Belperio JA et al., Circulating fibrocytes traffic to the lungs in response to CXCL12 and mediate fibrosis. J. Clin. Invest 2004 114: 438–446. [PubMed: 15286810]

26. Moore BB, Kolodsick JE, Thannickal VJ, Cooke K, Moore TA, Hogaboam C, Wilke CA et al., CCR2-mediated recruitment of fibrocytes to the alveolar space after fibrotic injury. Am. J. Pathol 2005 166: 675–684. [PubMed: 15743780]

27. Kao H-K, Chen B, Murphy GF, Li Q, Orgill DP **and** Guo L, Peripheral blood fibrocytes: enhancement of wound healing by cell proliferation, re-epithelialization, contraction, and angiogenesis. Ann. Surg 2011 254: 1066–1074. [PubMed: 21832942] **and**

28. Reilkoff RA, Bucala R **and** Herzog EL, Fibrocytes: emerging effector cells in chronic inflammation. Nat. Rev. Immunol 2011 11: 427–435. [PubMed: 21597472] **and**

29. Andersson-Sjöland A, de Alba CG, Nihlberg K, Becerril C, Ramírez R, Pardo A, Westergren-Thorsson G et al., Fibrocytes are a potential source of lung fibroblasts in idiopathic pulmonary fibrosis. Int. J. Biochem. Cell Biol 2008 40: 2129–2140. [PubMed: 18374622]

30. Mehrad B, Burdick MD **and** Strieter RM, Fibrocyte CXCR4 regulation as a therapeutic target in pulmonary fibrosis. Int. J. Biochem. Cell Biol 2009 41: 1708–1718. [PubMed: 19433312] **and**

31. Harris DA, Zhao Y, LaPar DJ, Emaminia A, Steidle JF, Stoler M, Linden J et al., Inhibiting CXCL12 blocks fibrocyte migration and differentiation and attenuates bronchiolitis obliterans in a murine heterotopic tracheal transplant model. J. Thorac. Cardiovasc. Surg 2013 145: 854–861. [PubMed: 22626514]

32. Reese C, Lee R, Bonner M, Perry B, Heywood J, Silver RM, Tourkina E et al., Fibrocytes in the fibrotic lung: altered phenotype detected by flow cytometry. Front. Pharmacol 2014 5: 141. [PubMed: 24999331]

33. Suga H, Rennert RC, Rodrigues M, Sorkin M, Glotzbach JP, Januszyk M, Fujiwara T et al., Tracking the elusive fibrocyte: identification and characterization of collagen-producing hematopoietic lineage cells during murine wound healing. Stem Cells 2014 32: 1347–1360. [PubMed: 24446236]
34. Furtado MB, Costa MW, Pranoto EA, Salimova E, Pinto AR, Lam NT, Park A et al., Cardiogenic genes expressed in cardiac fibroblasts contribute to heart development and repair. Circ. Res 2014 114: 1422–1434. [PubMed: 24650916]
35. Snider P, Standley KN, Wang J, Azhar M, Doetschman T **and** Conway SJ, Origin of cardiac fibroblasts and the role of periostin. Circ. Res 2009 105: 934–947. [PubMed: 19893021] **and**
36. Shi C, Jia T, Mendez-Ferrer S, Hohl TM, Serbina NV, Lipuma L, Leiner I et al., Bone marrow mesenchymal stem and progenitor cells induce monocyte emigration in response to circulating toll-like receptor ligands. Immunity 2011 34: 590–601. [PubMed: 21458307]
37. Ruddy MJ, Wong GC, Liu XK, Yamamoto H, Kasayama S, Kirkwood KL **and** Gaffen SL, Functional cooperation between interleukin-17 and tumor necrosis factor-alpha is mediated by CCAAT/enhancer-binding protein family members. J. Biol. Chem 2004 279: 2559–2567. [PubMed: 14600152] **and**
38. Holloway AF, Rao S, Chen X **and** Shannon Mes., Changes in chromatin accessibility across the GM-CSF promoter upon T cell activation are dependent on nuclear factor kappaB proteins. J. Exp. Med 2003 197: 413–423. [PubMed: 12591900] **and**
39. Johnson BV, Bert AG, Ryan GR, Condina A **and** Cockerill PN, Granulocyte-macrophage colony-stimulating factor enhancer activation requires cooperation between NFAT and AP-1 elements and is associated with extensive nucleosome reorganization. Mol. Cell. Biol 2004 24: 7914–7930. [PubMed: 15340054] **and**
40. Horiuchi K, Amizuka N, Takeshita S, Takamatsu H, Katsuura M, Ozawa H, Toyama Y et al., Identification and characterization of a novel protein, periostin, with restricted expression to periosteum and periodontal ligament and increased expression by transforming growth factor beta. J. Bone Miner. Res 1999 14: 1239–1249. [PubMed: 10404027]
41. Kanisicak O, Khalil H, Ivey MJ, Karch J, Maliken BD, Correll RN, Brody MJ et al., Genetic lineage tracing defines myofibroblast origin and function in the injured heart. Nat. Commun 2016 7: 12260. [PubMed: 27447449]
42. Bagchi RA, Wang R, Jahan F, Wigle JT **and** Czubryt MP, Regulation of scleraxis transcriptional activity by serine phosphorylation. J. Mol. Cell. Cardiol 2016 92: 140–148. [PubMed: 26883788] **and**
43. Nagpal V, Rai R, Place AT, Murphy SB, Verma SK, Ghosh AK **and** Vaughan DE, MiR-125b Is Critical for Fibroblast-to-Myofibroblast Transition and Cardiac Fibrosis. Circulation 2016 133: 291–301. [PubMed: 26585673] **and**
44. Rizvi F, DeFranco A, Siddiqui R, Negmadjanov U, Emelyanova L, Holmuhamedov A, Ross G et al., Chamber-specific differences in human cardiac fibroblast proliferation and responsiveness toward simvastatin. Am. J. Physiol. Cell Physiol 2016 311: C330–C339. [PubMed: 27335167]
45. Furtado MB, Nim HT, Boyd SE **and** Rosenthal NA, View from the heart: cardiac fibroblasts in development, scarring and regeneration. Development 2016 143: 387–397. [PubMed: 26839342] **and**
46. Moore-Morris T, Cattaneo P, Puceat M **and** Evans SM, Origins of cardiac fibroblasts. J. Mol. Cell. Cardiol 2016 91: 1–5. [PubMed: 26748307] **and**
47. Barin JG, Baldeviano GC, Talor MV, Wu L, Ong S, Fairweather D, Bedja D et al., Fatal eosinophilic myocarditis develops in the absence of IFN-gamma and IL-17A. J. Immunol 2013 191: 4038–4047. [PubMed: 24048893]
48. Barin JG, Talor MV, Baldeviano, Gan., Kimura, M., Rose, N. R. and Čiháková D., Mechanisms of IFN gamma regulation of autoimmune myocarditis. Exp. Mol. Pathol 2010 89: 83–91. [PubMed: 20599938]
49. Cihakova D, Barin JG, Afanasyeva M, Kimura M, Fairweather D, Berg M, Talor MV et al., Interleukin-13 protects against experimental autoimmune myocarditis by regulating macrophage differentiation. Am. J. Pathol 2008 172: 1195–1208. [PubMed: 18403598]

50. Diny NL, Baldeviano Gan., Talor MV, Barin JG, Ong S, Bedja D, Hays AG et al., Eosinophil-derived IL-4 drives progression of myocarditis to inflammatory dilated cardiomyopathy. J. Exp. Med 2017 214: 943–957. [PubMed: 28302646]
51. Diny NL, Hou X, Barin JG, Chen G, Talor MV, Schaub J, Russell SD et al., Macrophages and cardiac fibroblasts are the main producers of eotaxins and regulate eosinophil trafficking to the heart. Eur. J. Immunol 2016 46: 2749–2760. [PubMed: 27621211]
52. Cakouros D, Cockerill PN, Bert AG, Mital R, Roberts DC **and** Shannon MF, A NF-kappa B/Sp1 region is essential for chromatin remodeling and correct transcription of a human granulocyte-macrophage colony-stimulating factor transgene. J. Immunol 2001 167: 302–310. [PubMed: 11418664] **and**
53. Cockerill PN, Mechanisms of transcriptional regulation of the human IL-3/GM-CSF locus by inducible tissue-specific promoters and enhancers. Crit. Rev. Immunol 2004 24: 385–408. [PubMed: 15777160]
54. Duncliffe KN, Bert AG, Vadas MA **and** Cockerill PN, A T cell-specific enhancer in the interleukin-3 locus is activated cooperatively by Oct and NFAT elements within a DNase I-hypersensitive site. Immunity 1997 6: 175–185. [PubMed: 9047239] **and**
55. Gaffen SL, Structure and signalling in the IL-17 receptor family. Nat. Rev. Immunol 2009 9: 556–567. [PubMed: 19575028]
56. Gaffen SL, Jain R, Garg AV **and** Cua DJ, The IL-23-IL-17 immune axis: from mechanisms to therapeutic testing. Nat. Rev. Immunol 2014 14: 585–600. [PubMed: 25145755] **and**
57. Wurster AL, Precht P **and** Pazin MJ, NF-kappaB and BRG1 bind a distal regulatory element in the IL-3/GM-CSF locus. Mol. Immunol 2011 48: 2178–2188. [PubMed: 21831442] **and**
58. Nguyen HN, Noss EH, Mizoguchi F, Huppertz C, Wei KS, Watts GFM **and** Brenner MB, Autocrine Loop Involving IL-6 Family Member LIF, LIF Receptor, and STAT4 Drives Sustained Fibroblast Production of Inflammatory Mediators. Immunity 2017 46: 220–232. [PubMed: 28228280] **and**
59. Keegan PM, Anbazhakan S, Kang B, Pace BS **and** Platt MO, Biomechanical and biochemical regulation of cathepsin K expression in endothelial cells converge at AP-1 and NF-kappaB. Biol. Chem 2016 397: 459–468. [PubMed: 26760306] **and**
60. Koga Y, Hisada T, Ishizuka T, Utsugi M, Ono A, Yatomi M, Kamide Y et al., CREB regulates TNF-alpha-induced GM-CSF secretion via p38 MAPK in human lung fibroblasts. Allergol. Int 2016 65: 406–413. [PubMed: 27118435]
61. Maekawa Y, Anzai T, Yoshikawa T, Sugano Y, Mahara K, Kohno T, Takahashi T et al., Effect of granulocyte-macrophage colony-stimulating factor inducer on left ventricular remodeling after acute myocardial infarction. J. Am. Coll. Cardiol 2004 44: 1510–1520. [PubMed: 15464336]
62. Kaur H, Takefuji M, Ngai CY, Carvalho J, Bayer J, Wietelmann A, Poetsch A et al., Targeted ablation of periostin-expressing activated fibroblasts prevents adverse cardiac remodeling in mice. Circ. Res 2016 118: 1906–1917. [PubMed: 27140435]
63. Dominici M, Le Blanc K, Mueller I, Slaper-Cortenbach I, Marini FC, Krause DS, Deans RJ et al., Minimal criteria for defining multipo-tent mesenchymal stromal cells. The International Society for Cellular Therapy position statement. Cytotherapy 2006 8: 315–317. [PubMed: 16923606]
64. De Schauwer C, Meyer E, Van de Walle GR **and** Van Soom A, Markers of stemness in equine mesenchymal stem cells: a plea for uniformity. Theriogenology 2011 75: 1431–1443. [PubMed: 21196039] **and**
65. Monsanto MM, White KS, Kim T, Wang BJ, Fisher K, Ilves K, Khalafalla FG et al., Concurrent isolation of 3 distinct cardiac stem cell populations from a single human heart biopsy. Circ. Res 2017 121: 113–124. [PubMed: 28446444]
66. Chong JJH, Forte E **and** Harvey RP, Developmental origins and lineage descendants of endogenous adult cardiac progenitor cells. Stem Cell Res 2014 13(3 Pt B): 592–614. [PubMed: 25459343] **and**
67. Wang X, Hu Q, Nakamura Y, Lee J, Zhang G, From AHL **and** Zhang J, The role of the sca-1^{+}/CD31- cardiac progenitor cell population in postinfarction left ventricular remodeling. Stem Cells 2006 24: 1779–1788. [PubMed: 16614004] **and**

68. Valente M, Nascimento DS, Cumano A **and** Pinto-do-ó P, Sca-1^{+} cardiac progenitor cells and heart-making: a critical synopsis. Stem Cells Dev. 2014 23: 2263–2273. [PubMed: 24926741] **and**
69. Wang H, Chen H, Feng B, Wang X, He X, Hu R, Yin M et al., Isolation and characterization of a Sca-1^{+}/CD31- progenitor cell lineage derived from mouse heart tissue. BMC Biotechnol. 2014 14: 75. [PubMed: 25106452]
70. Razeghi P, Young ME, Alcorn JL, Moravec CS, Frazier OH **and** Taegtmeyer H, Metabolic gene expression in fetal and failing human heart. Circulation 2001 104: 2923–2931. [PubMed: 11739307] **and**
71. Yu JJ, Ruddy MJ, Conti HR, Boonanantanasarn K **and** Gaffen SL, The interleukin-17 receptor plays a gender-dependent role in host protection against Porphyromonas gingivalis-induced periodontal bone loss. Infect. Immun 2008 76: 4206–4213. [PubMed: 18591228] **and**
72. El Malki K, Karbach SH, Huppert J, Zayoud M, Reißig S, Schüler R, Nikolaev A et al., An alternative pathway of imiquimod-induced psoriasis-like skin inflammation in the absence of interleukin-17 receptor a signaling. J. Invest. Dermatol 2013 133: 441–451. [PubMed: 22951726]
73. Lindsley A, Snider P, Zhou H, Rogers R, Wang J, Olaopa M, Kruzynska-Frejtag A et al., Identification and characterization of a novel Schwann and outflow tract endocardial cushion lineage-restricted periostin enhancer. Dev. Biol 2007 307: 340–355. [PubMed: 17540359]
74. Pummerer CL, Luze K, Grässl G, Bachmaier K, Offner F, Burrell SK, Lenz DM et al., Identification of cardiac myosin peptides capable of inducing autoimmune myocarditis in BALB/c mice. J. Clin. Invest 1996 97: 2057–2062. [PubMed: 8621795]
75. Čiháková D, Sharma RB, Fairweather D, Afanasyeva M **and** Rose NR, Animal models for autoimmune myocarditis and autoimmune thyroiditis. Methods Mol. Med 2004 102: 175–193. [PubMed: 15286386] **and**
76. Yang F, Liu Y-H, Yang X-P, Xu J, Kapke A **and** Carretero OA, Myocardial infarction and cardiac remodelling in mice. Exp. Physiol 2002 87: 547–555. [PubMed: 12481929] **and**
77. Takagawa J, Zhang Y, Wong ML, Sievers RE, Kapasi NK, Wang Y, Yeghiazarians Y et al., Myocardial infarct size measurement in the mouse chronic infarction model: comparison of area- and length-based approaches. J. Appl. Physiol (1985) 2007 102: 2104–2111.
78. Afanasyeva M, Georgakopoulos D, Belardi DF, Ramsundar AC, Barin JG, Kass DA **and** Rose NR, Quantitative analysis of myocar-dial inflammation by flow cytometry in murine autoimmune myocarditis: correlation with cardiac function. Am. J. Pathol 2004 164: 807–815. [PubMed: 14982835] **and**
79. Fu K, Sun X, Wier EM, Hodgson A, Liu Y, Sears CL **and** Wan F, Sam68/KHDRBS1 is critical for colon tumorigenesis by regulating genotoxic stress-induced NF-kappaB activation. Elife 2016 5 pii: e15018. [PubMed: 27458801] **and**
80. Wan F, Anderson Dic., Barnitz RA, Snow A, Bidere N, Zheng L, Hegde V et al., Ribosomal protein S3: a KH domain subunit in NF-kappaB complexes that mediates selective gene regulation. Cell 2007 131: 927–939. [PubMed: 18045535]
81. Livak KJ **and** Schmittgen TD, Analysis of relative gene expression data using real-time quantitative PCR and the 2(-Delta Delta C(T)) Method. Methods 2001 25: 402–408. [PubMed: 11846609]

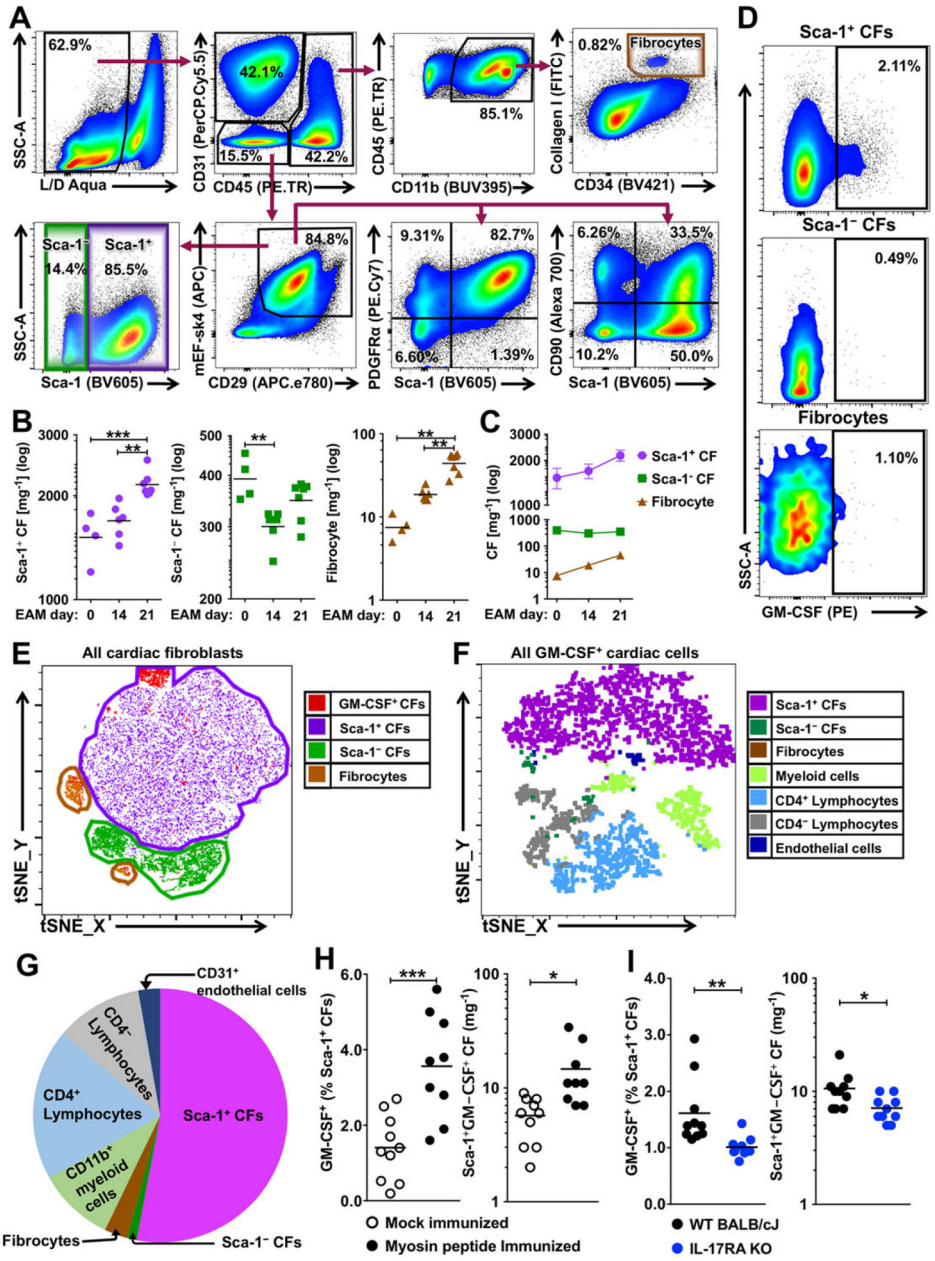

Figure 1.

Sca-1$^+$ cardiac fibroblasts are potent GM-CSF-producers during cardiac inflammation. Cardiac fibroblasts were harvested from wild type BALB/c mice with EAM on days 0, 14 or 21 for flow cytometry analysis. (A) Representative flow cytometry plots depict gating strategies for cardiac fibroblast subsets. (B) Flow cytometric quantification of the numbers of cardiac fibroblast subsets per mg cardiac tissue at different time points after EAM induction. (n = 4 for EAM day 0 group; n = 6 for EAM day 14 group; n = 7 for EAM day 21 group; CF cardiac fibroblast) (C) Demonstration of cell number changes in cardiac fibroblast subsets after EAM induction. (D) Representative flow cytometry= plots showing GM-CSF staining of cardiac fibroblast subsets on day 21 of EAM. (E and F) Representative t-SNE

clustering plots of (E) cardiac fibroblast subsets and GM-CSF-positive cardiac fibroblasts or (F) all GM-CSF-positive cardiac cells on day 21 of EAM using t-SNE dimensionality reduction algorithm plugin in FlowJo 10.4.2 (FlowJo, LLC). (G) Relative frequency of different cell populations out of all GM-CSF-positive cells in the hearts on day 21 of EAM. (H) Frequency and number of GM-CSF-positive Sca-1^+ cardiac fibroblasts per mg cardiac tissue in immunized mice ($n = 9$) versus mock-immunized mice ($n = 10$) on day 21 of EAM. (I) Frequency and number of GM-CSF-positive Sca-1^+ cardiac fibroblasts per mg cardiac tissue in immunized WT mice and *Il17ra*−/− mice on day 21 of EAM ($n = 10$ per group). Data are representative of three independent experiments (A–I). Groups were compared using one-way ANOVA followed by Tukey's post-test (B) or Student's *t*-test (H–I). $^{*}p < 0.05$; $^{**}p < 0.01$; $^{***}p < 0.001$.

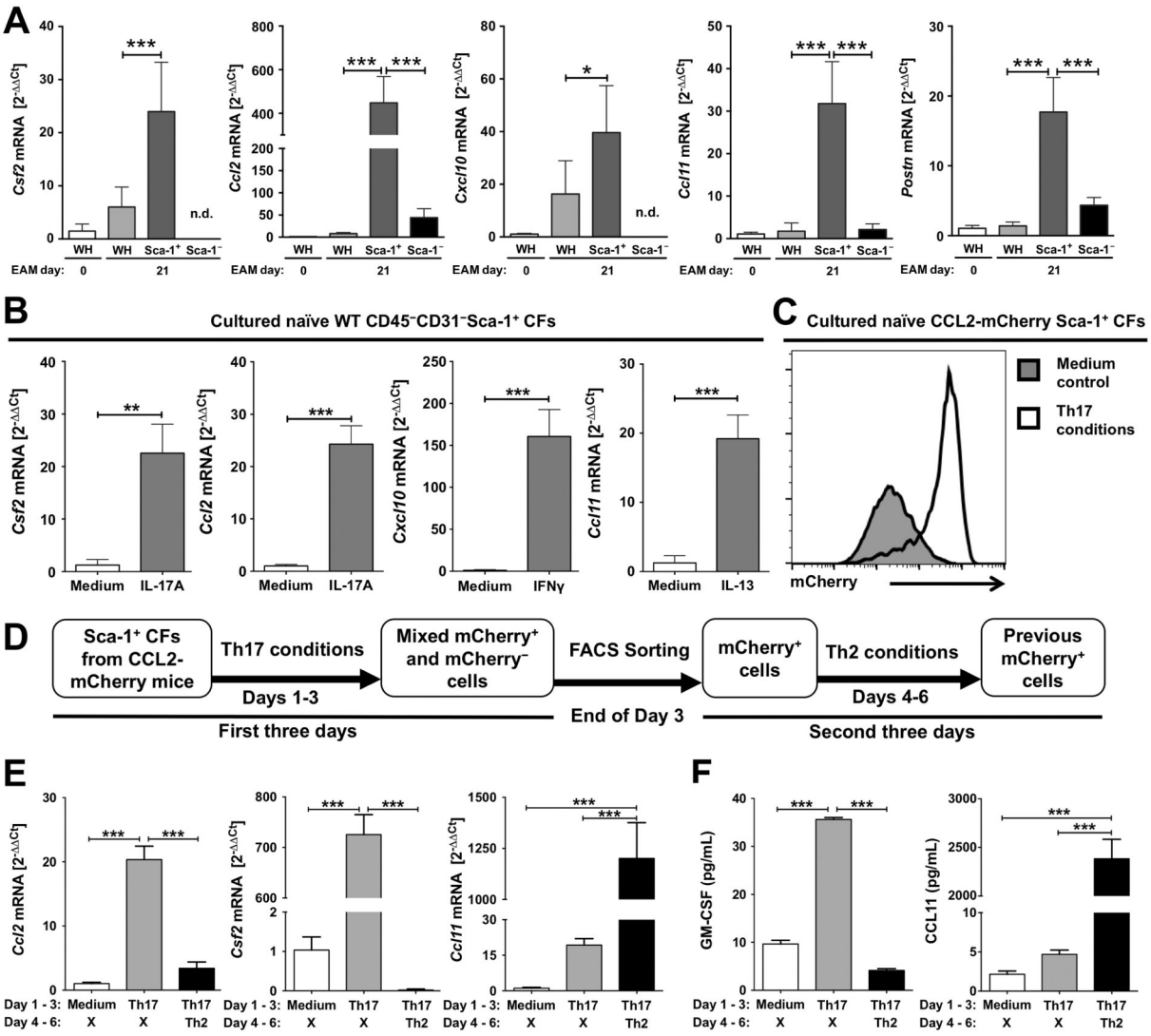

Figure 2.

Sca-1$^+$ cardiac fibroblasts are potent producers of different cytokines and chemokines and are plastic in response to environment changes. (A) The mRNA expression levels of *Csf2, Ccl2, Cxcl10, Ccl11* and *Postn* in na¨ıve mouse heart homogenates, EAM day 21 mouse heart homogenates and FACS-sorted Sca-1$^+$ and Sca-1$^-$ cardiac fibroblasts from EAM day 21 mouse hearts (n =5 per group; n.d. not detected; WH = whole heart homogenate). Expression levels were analyzed by qPCR ($2^{-\Delta\Delta Ct}$ values relative to *Gapdh* expression levels and=na¨ıve whole heart transcripts). (B) The mRNA expression levels of *Csf2, Ccl2, Cxcl10* and *Ccl11* in in vitro cultured Sca-1$^+$ cardiac fibroblasts stimulated with IL-17A, IL-13, IFN-γ, or unstimulated (control). Expression levels were analyzed by qPCR ($2^{-\Delta\Delta Ct}$ values relative to *Gapdh* expression levels and unstimulated controls). (C) Representative histogram of mCherry (CCL2) expression in cultured Sca-1$^+$ cardiac fibroblasts under Th17 conditions or unstimulated. (D) Schematic of the experiment procedures for all data showing in E–F. (E) Expression levels of *Ccl2*, *Csf2* and *Ccl11* mRNA in cells harvested on day 3 or day 6. Expression levels were analyzed by qPCR ($2^{-\Delta\Delta Ct}$ values relative to *Gapdh*

expression levels and unstimulated controls). (F) Protein concentrations of secreted CCL11 and GM-CSF in the culture supernatant harvested on day 3 or day 6 were measured by quantitative sandwich ELISA. Data are shown as mean + SD of five mice per group (A) or of technical triplicates (B, E–F). Data are representative of three indepen dent experiments (A–F). Groups were compared using one-way ANOVA followed by Tukey's post-test (A, E–F) or Student's *t*-test (B). $^{**}p < 0.01$; $^{***}p < 0.001$.

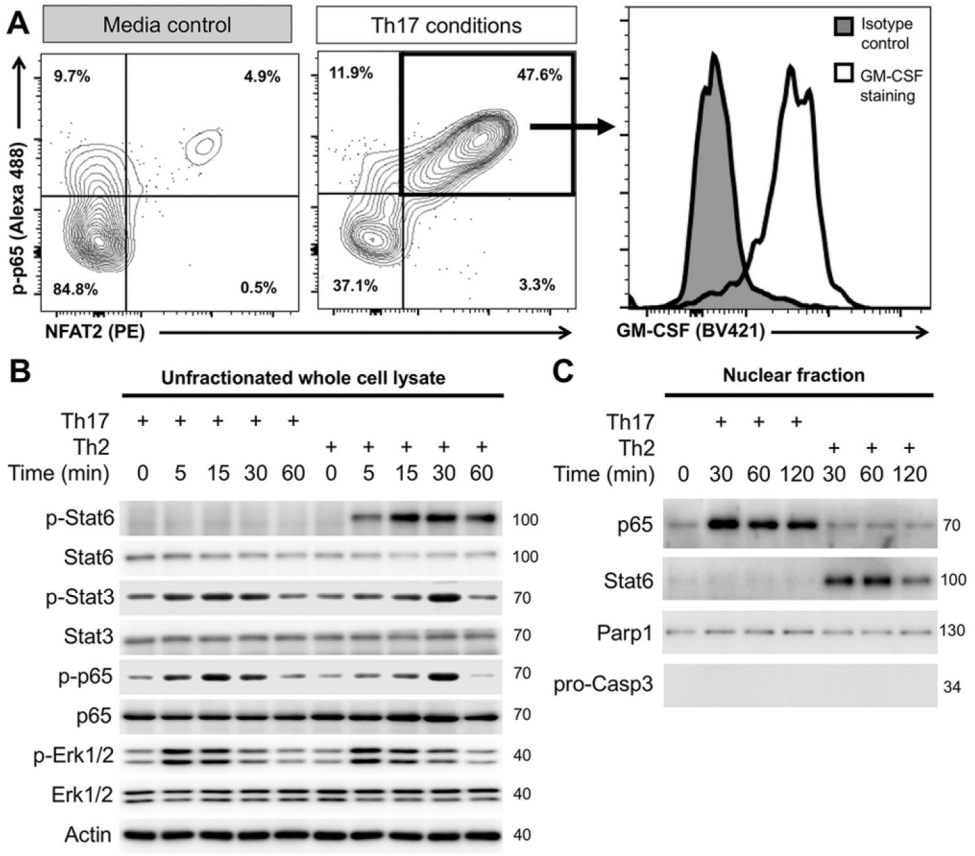

Figure 3.

IL-17A induces GM-CSF production in Sca-1$^+$ cardiac fibroblasts through synergistic activation of NF-κB and NFAT2. (A–C) Sca-1$^+$ cardiac fibroblasts were MACS-sorted from naïve WT mouse hearts and cultured under Th17 conditions (IL-17A TNF-α), Th2 conditions (IL-13) or unstimulated (control) for two days (A) or for multiple time points (B–C). (A) Representative flow cytometry plots showing phosphorylated p-65 (pp65)-positive and/or NFAT2-positive Sca-1$^+$ cardiac fibroblasts and representative histogram showing their GM-CSF expression. (B) Immunoblots showing the detection of total or phosphorylated Stat6, Stat3, p65 and Erk1/2 in whole cell lysate. (C) Immunoblots showing the detection of p65, Stat6, Parp1 (nuclear positive control) and pro-Caspase 3 (nuclear negative control) in the nuclear fraction of Sca-1 cardiac fibroblasts with/without stimulation. Data are representative of three independent experiments (A–C).

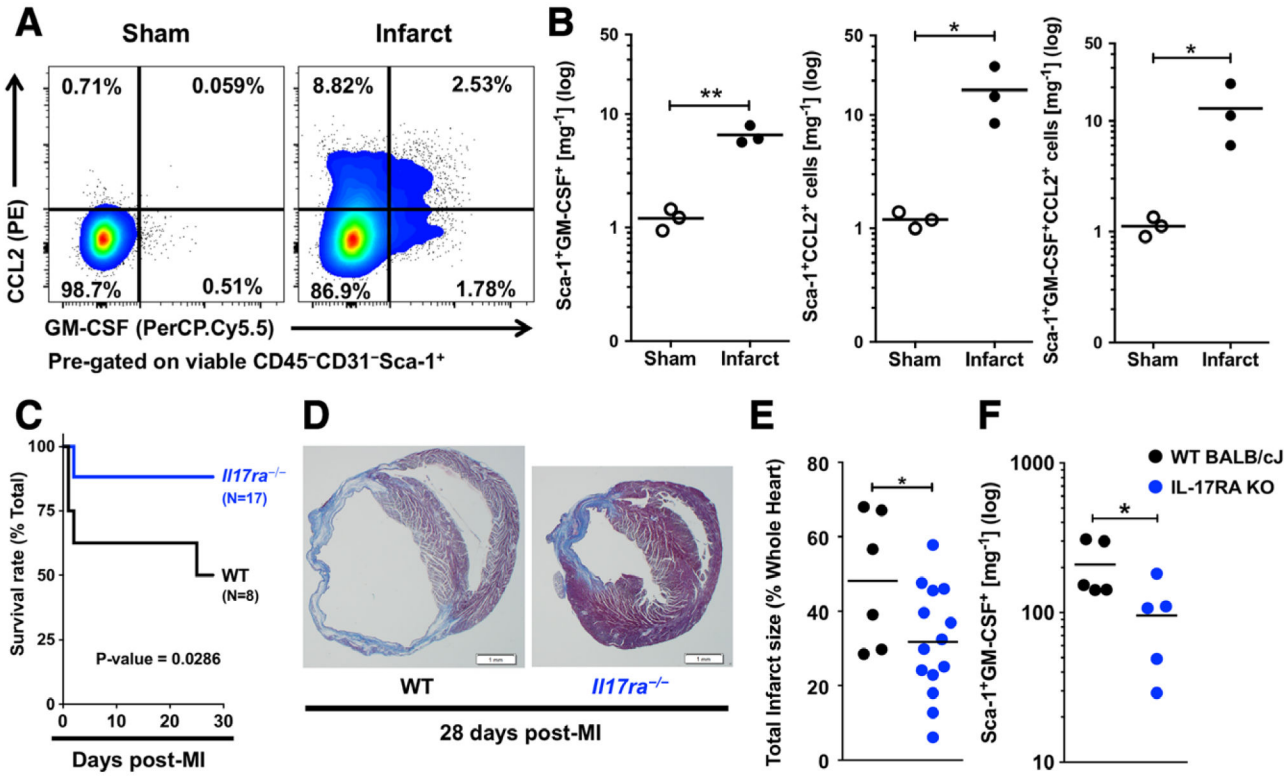

Figure 4.

IL-17A signaling ablation leads to less GM-CSF-positive Sca-1$^+$ cardiac fibroblasts and protects mice from post-MI heart failure and death. (A) Representative flow cytometry plots showing GM-CSF- and CCL2-positive Sca-1$^+$ cardiac fibroblasts in infarcted and sham-operated mouse hearts on day 2 post-MI. Cells were pre-gated on viable CD45$^-$CD31$^-$Sca-1$^+$ cardiac cells. (B) Flow cytometric quantification of GM-CSF$^+$, CCL2$^+$ and GM-CSF$^+$CCL2$^+$ Sca-1$^+$ cardiac fibroblasts per mg cardiac tissue of infarcted or sham-operated WT mice (n =3 per group). (C) Kaplan-Meier survival curve of WT mice (n = 8) and *Il17ra*$^{-/-}$ mice (n = 17) on day 28 post-MI. (D) images Representative of Masson's trichrome stained histology slides of the cross-sections at the middle of the hearts from WT and *Il17ra*$^{-/-}$ mice showing the expansion of the infarct area and the dilation of the left ventricles on day 28 post-MI. (Scalebar, 1mm) (E) Calculated total infarct sizes of WT mice (n = 6) and *Il17ra*$^{-/-}$ mice (n 14) on day 28 post-MI. (F) Flow cytometric quantification of GM-CSF-positive Sca-1$^+$ cardiac fibroblasts per mg cardiac tissue in WT and *Il17ra* $^{-/-}$=mice on day 2 post-MI (n = 5 per group). Data are representative of three independent experiments (A–F). Groups were compared using Student's t-test (B, E–F) or Long-rank (Mantel-Cox) test (C). $^*p < 0.05$; $^{**}p < 0.01$.

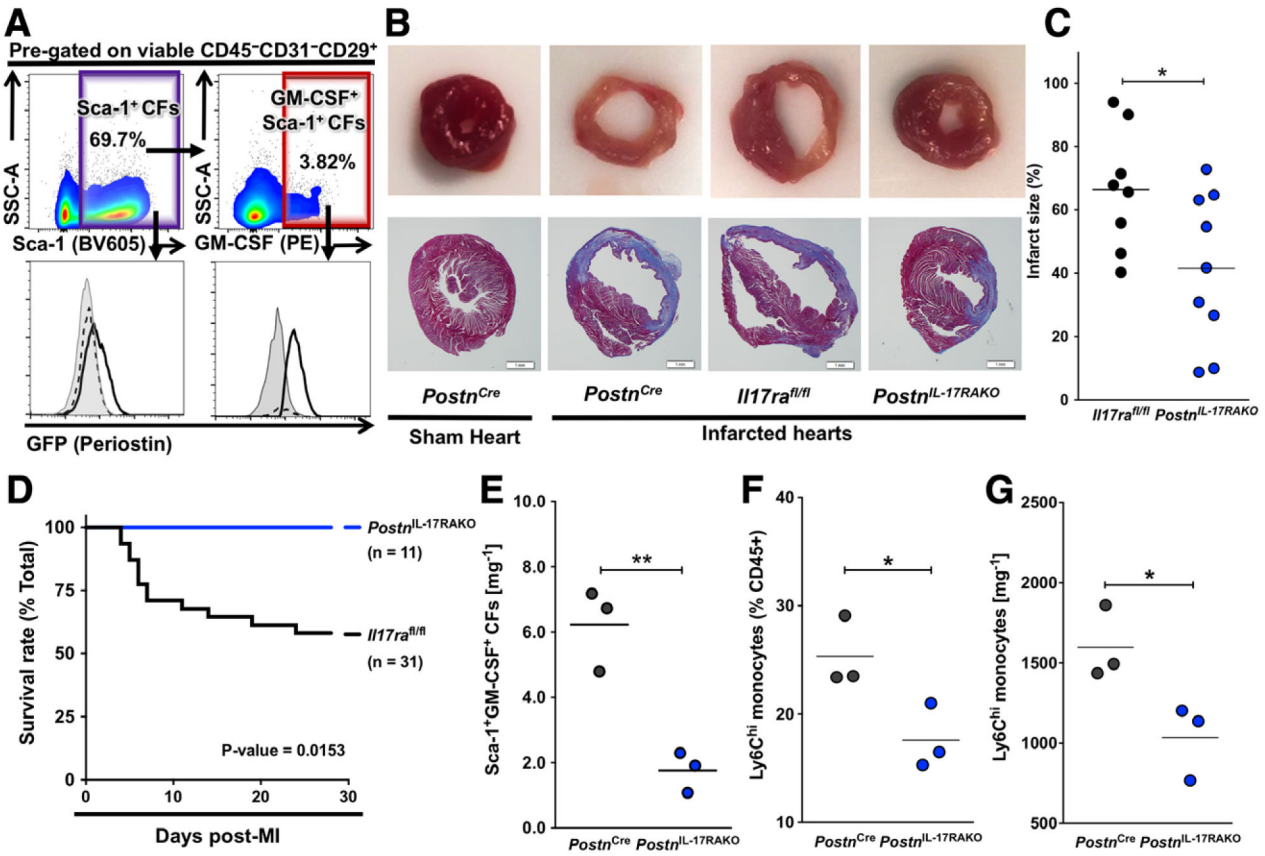

Figure 5.

GM-CSF-positive Sca-1$^+$ cardiac fibroblasts express periostin post-MI and specific IL-17RA ablation in periostin$^+$ cardiac fibroblasts protects mice from post-MI heart failure and death. (A) Representative flow cytometry plots showing Sca-1$^+$ and GM-CSF$^+$Sca-1$^+$ cardiac fibroblasts and representative histograms of their GFP (periostin) expression in infarcted WT mouse hearts (gray shadowed), sham (black dashed line) and infarcted (black solid line) *Postn*$^{Cre/eGFP}$ mouse hearts on day 2 post-MI. Cells were pre-gated on viable CD45$^-$CD31$^-$CD29$^+$ cells. (B) Representative images of Masson's trichrome stained histology slides of the cross-sections at the middle of the hearts from sham and infarcted *Postn*^{Cre}, infarcted *Il17ra*$^{fl/fl}$ and infarcted *Postn*^{Cre}*Il17ra*$^{fl/fl}$ mice on day 7 post-MI (*Postn*^{Cre}*Il17ra*$^{fl/fl}$ mice were labeled in this Figure as *Postn*$^{IL-17RAKO}$) showing the expansion of the infarct area and the dilation of the left ventricle of the infarcted mouse hearts. (Scalebar, 1mm) (C) Calculated total infarct sizes of infarcted *Il17ra*$^{fl/fl}$ mice (n = 8) and *Postn*^{Cre}*Il17ra*$^{fl/fl}$ mice (n =9) on day 7 post-MI. (D) Kaplan-Meier survival analysis of infarcted *Il17ra*$^{fl/fl}$ mice (n = 31) and *Postn*^{Cre}*Il17ra*$^{fl/fl}$ mice (n = 11) on day 28 post-MI. (E) Flow cytometric quantification of GM-CSF-positive Sca-1$^+$ cardiac fibroblasts per mg cardiac tissue in *Postn*^{Cre} and *Postn*^{Cre}*Il17ra*$^{fl/fl}$ mice on day 4 post-MI (n = 3 per group). (F-G) Flow cytometric quantification of the frequency (F) and the number (G) of Ly6C^{hi} monocytes per mg cardiac tissue in *Postn*^{Cre} and *Postn*^{Cre}*Il17ra*$^{fl/fl}$ mice on day 4 post-MI (n = 3 per group). "*Postn*$^{IL-17RAKO}$" stands for "*Postn*^{Cre}*Il17ra*$^{fl/fl}$ mice". "CFs" stands for "cardiac fibroblasts". Data are representative of three independent = experiments (A–G).

Groups were compared using Student's *t*-test (C, E–G) or Long-rank (Mantel-Cox) test (D). $^{*}p < 0.05$, $^{**}p < 0.01$.

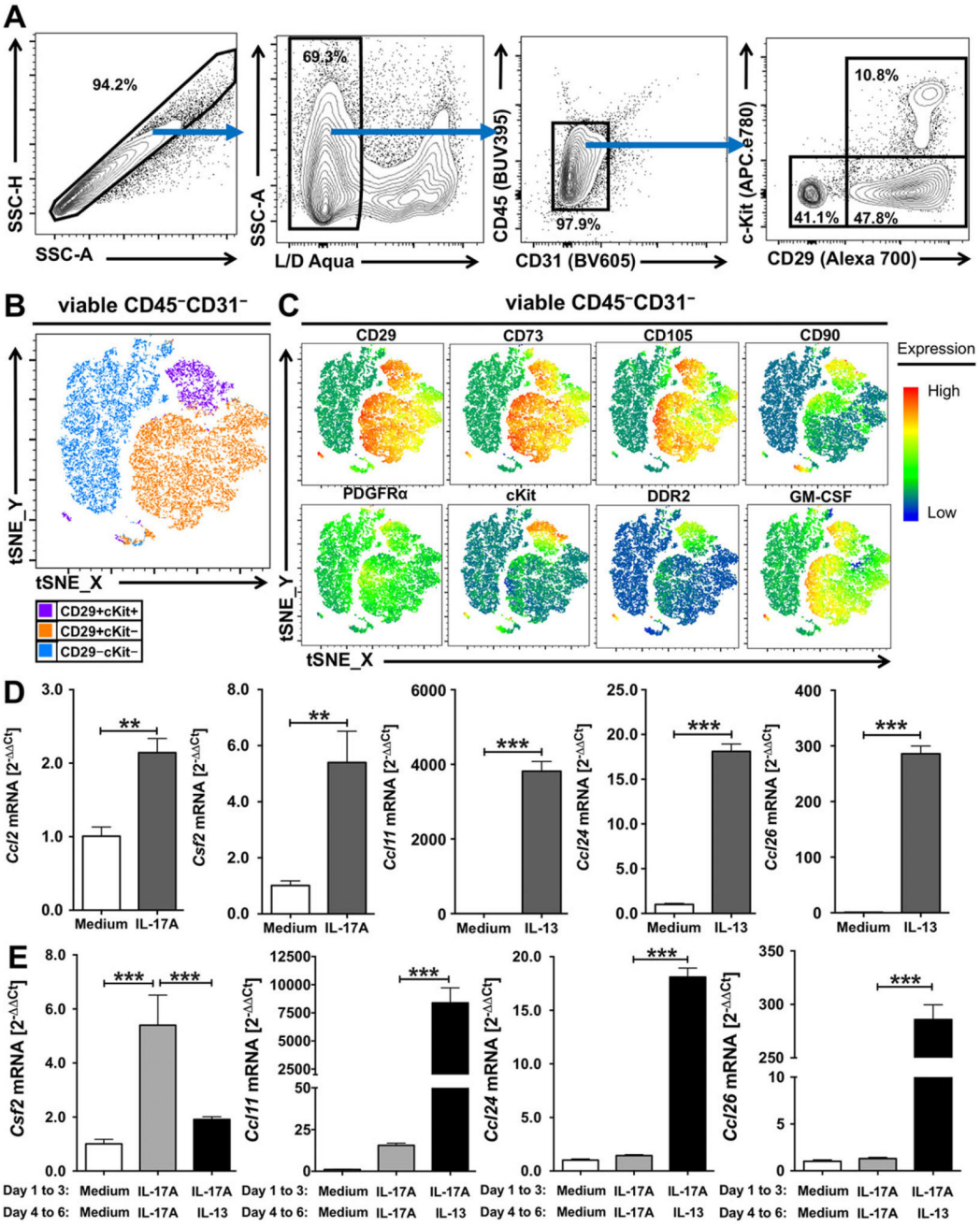

Figure 6.

GM-CSF-expressing cardiac fibroblast subset was found in human cardiac fibroblasts and exhibits similar functional plasticity. (A) Representative flow cytometry plots showing the gating strategies for cultured human primary cardiac fibroblasts. (B) Representative t-SNE clustering plots of three human cardiac fibroblast subsets using t-SNE dimensionality reduction algorithm plugin in FlowJo 10.4.2 (FlowJo, LLC). (C) Representative expression heat maps of cell surface markers, CD29, CD73, CD105, CD90, PDGFRα, cKit, DDR2 and GM-CSF expression in human cardiac fibroblasts using t-SNE dimensionality reduction algorithm plugin in FlowJo 10.4.2 (FlowJo, LLC). (D–E) The mRNA expression levels of

CCL2, *CSF2*, *CCL11*, *CCL24* and *CCL26* of human primary cardiac fibroblasts cultured under IL-17A, IL-13 or unstimulated (control) for three days (D) or washed and recultured again with/without change of stimuli for another three days (E). The mRNA expression levels were analyzed by qPCR ($2^{-\Delta\Delta Ct}$ values relative to *HPRT1* expression levels and unstimulated controls). Data are shown as mean SD of technical triplicates and are representative of three independent experiments (D–E). Groups were compared using Student's t test (D) or $^{+}$using one-way ANOVA followed by Tukey's post-test (E). $^{**}p < 0.01$; $^{***}p < 0.001$.

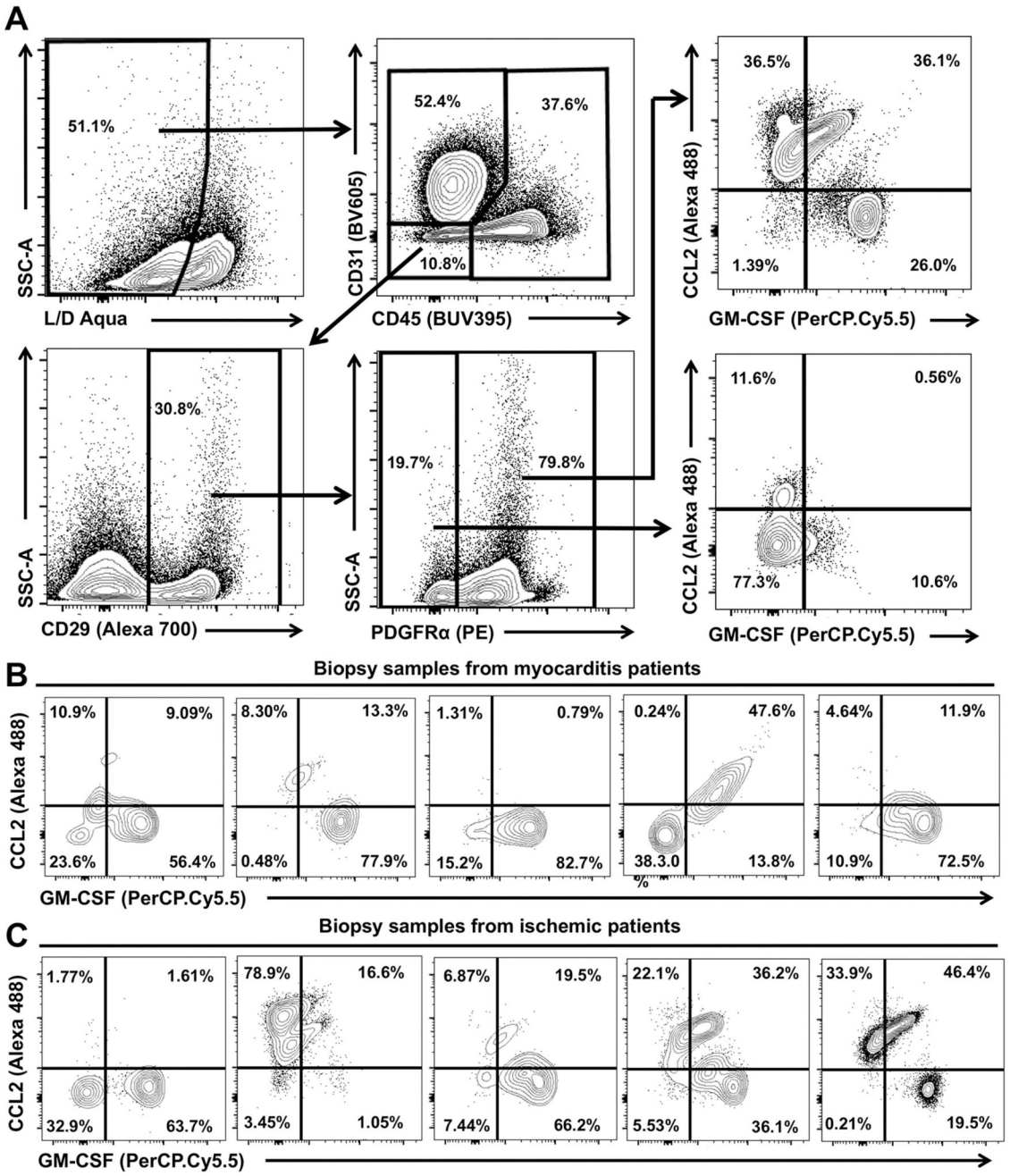

Figure 7.

Human cardiac fibroblasts from heart failure patients produce GM-CSF and CCL2. (A) Representative flow cytometry plots of the concatenated sample showing gating strategy for human $CD45^{-}CD31^{-}CD29^{+}PDGFR\alpha^{+}$ cardiac fibroblasts and flow cytometry plots showing GMCSF and CCL2 expressions for $PDGFR\alpha^{+}$ and $PDGFR\alpha^{-}$ cardiac fibroblasts from the heart biopsies of myocarditis or ischemic heart failure patients. (B) Representative flow cytometry plots showing GM-CSF and CCL2 expression by $PDGFR\alpha^{+}$ cardiac fibroblasts from heart biopsies of five myocarditis heart failure patients. (C) Representative flow cytometry plots showing GM-CSF and CCL2 expression by $PDGFR\alpha^{+}$ cardiac

fibroblasts from heart biopsies of five ischemic heart failure patients. Data are from 5 myocarditis heart failure patients and 5 ischemic heart failure patients.